An Approximate Maximum Likelihood Method for the Joint Estimation of Range and Doppler of Multiple Targets in OFDM-Based Radar Systems

Michele Mirabella, *Graduate Student Member, IEEE*, Pasquale Di Viesti, *Graduate Student Member, IEEE*, Alessandro Davoli, *Graduate Student Member, IEEE*, and Giorgio M. Vitetta, *Senior Member, IEEE*

***Abstract*— In this manuscript, an innovative method for the detection and the estimation of multiple targets in a radar system employing orthogonal frequency division multiplexing is illustrated. The core of this method is represented by a novel algorithm for detecting multiple superimposed two-dimensional complex tones in the presence of noise and estimating their parameters. This algorithm is based on a maximum likelihood approach and combines a single tone estimator with a serial cancellation procedure. Our numerical results lead to the conclusion that the developed method can achieve a substantially better accuracy-complexity trade-off than various related techniques in the presence of closely spaced targets.**

***Index Terms*— Dual-function radar-communication, frequency estimation, harmonic retrieval, maximum likelihood estimation, orthogonal frequency division multiplexing, radar processing.**

I. Introduction

WIRELESS communication and radar sensing have been advancing independently for many years, even though they share various similarities in terms of both signal processing and system architecture. In the last few years, substantial research efforts have been devoted to the design of wireless systems able to perform *communication and radar* functions jointly. The interest in this class of systems, that accomplish *joint communication and sensing* (JCAS), has been motivated by the advantages they offer in terms of device size, power consumption, cost and efficiency radio spectrum usage with respect to traditional wireless systems in various applications [1].

In this manuscript we focus on a *communication-centric* JCAS approach, where the radar sensing function can be considered as an add-on to the given communication system. More specifically, we take into consideration a *single-input single-output* (SISO) JCAS system employing *orthogonal frequency division multiplexing* (OFDM); this modulation format has been adopted in various wireless communication standards, thanks to its robustness to multipath fading and to its relatively simple synchronization [2].

In the technical literature, *direct* and *indirect sensing* methods for target detection and estimation are available for OFDM-based JCAS systems. Generally speaking, *direct sensing methods* extract target information from the received signal without compensating for the effect of the data payload it conveys [1], [3] and typically exploit computationally intensive *compressed sensing* (CS) techniques. *Indirect estimation methods*, instead, require estimating the communication channel and, consequently, compensating for the contribution due to channel symbols (e.g., see [4, eq. (20)]). Indirect sensing methods can be divided in: 1) *discrete Fourier transform* (DFT)-based or *correlation-based* methods (i.e., methods based on the *matched filter*, MF, concept) [5], [6], [7]; 2) subspace methods [3], [8], [9]; 3) *maximum likelihood* (ML) based methods [10], [11], [12], [13].

Correlation-based and DFT-based methods for joint range-velocity estimation exploit prior knowledge of the received signal and, even if conceptually simple and computationally efficient, may generate poor radar images in the presence of closely spaced targets or strong clutter around them [14]. Such methods can be outperformed by subspace methods, like the well known *multiple signal classification* (MUSIC) algorithm and the *estimation of signal parameters via rotational invariant technique* (ESPRIT) at the price, however, of a significantly larger computational complexity [8]. An accuracy comparable to that of subspace methods can be achieved through various ML-based algorithms, which also require a significant computational effort. Relevant contributions to this field concern: 1) the use of the *amplitude weighted linearly constrained minimum variance* (AW-LCMV) method for estimating the parameters of multiple targets [10]; 2) the adoption of an *alternating maximization* approach to mitigate the computational complexity of ML estimation [11]; 3) the development of an iterative non-linear *kernel least mean*

Manuscript received 19 July 2022; revised 2 December 2022 and 31 March 2023; accepted 19 May 2023. Date of publication 29 May 2023; date of current version 16 August 2023. The associate editor coordinating the review of this article and approving it for publication was R. Tandon. *(Corresponding author: Giorgio M. Vitetta.)*

The authors are with the Department of Engineering "Enzo Ferrari", University of Modena and Reggio Emilia, 41125 Modena, Italy, and also with Consorzio Nazionale Interuniversitario per le Telecomunicazioni (CNIT), 43124 Parma, Italy (e-mail: michele.mirabella@unimore.it; pasquale.diviesti@unimore.it; alessandro.davoli@unimore.it; giorgio.vitetta@unimore.it).

Color versions of one or more figures in this article are available at https://doi.org/10.1109/TCOMM.2023.3280562.

Digital Object Identifier 10.1109/TCOMM.2023.3280562

square (KLMS) based technique for the estimation of target range [12]; 4) the derivation of a ML method, based on a kinematic model of detected targets, for estimating target speed [13].

The work illustrated in this manuscript has been motivated by our interest in extending our ML-based estimator of multiple overlapped complex exponentials developed in [15] to a *two-dimensional* (2D) scenario, and to investigate the application of the resulting algorithm to the detection of multiple targets and the estimation of their range and Doppler in an OFDM-based JCAS system. The contribution provided by this manuscript is threefold and can be summarised as follows:

1) A novel iterative DFT-based algorithm, called *complex single frequency-delay estimation* (CSFDE), is developed for the ML estimation of a single 2D complex tone. This estimator is based on the *periodogram method* for coarse frequency estimation and on a new iterative algorithm for the estimation of frequency residuals and complex amplitude. The last algorithm requires the evaluation of multiple *symplectic Fourier transforms* (SFTs), but, unlike other estimation techniques, does not need a prior knowledge of the overall number of targets. Moreover, its derivation is based on: a) a new approximate expression of the ML metric; b) the exploitation of the *alternating minimization* technique.

2) A novel recursive algorithm, called *complex single frequency-delay estimation and cancellation* (CSFDEC), for the estimation of the parameters of multiple superimposed 2D tones is derived. This algorithm, that combines the CSFDE algorithm with a serial cancellation & refinement procedure, is applied to target range and Doppler estimation in the considered JCAS system.

3) The accuracy of the CSFDEC algorithm is assessed by extensive computer simulations and compared with that achieved by various related algorithms available in the technical literature.

Our numerical results lead to the conclusion that the CSFDEC algorithm outperforms all the other related estimators in terms of probability of convergence, and achieves similar or better accuracy in all the considered scenarios; in particular, it is able to reliably operate in the presence of multiple closely-spaced targets in scenarios in which DFT-based methods, subspace methods and other ML-based methods fail. In addition, the computational requirements of the CSFDEC algorithm are quite limited; this is due to the fact that it exploits a DFT-based method (namely, the CSFDE algorithm) and a mathematically simple serial cancellation & refinement procedure, that unlike ML-based and subspace methods, does not require matrix inversions and eigendecompositions. Moreover, the CSFDEC algorithm is an *off-grid* algorithm since, unlike most of the ML-based methods available in the technical literature, does not make use of a search grid in frequency estimation; this makes its application substantially easier than *on-grid* algorithms.

The remaining part of this manuscript is organized as follows. In Section II, the processing accomplished in an OFDM-based radar system is summarised and the model of the signal feeding the CSFDEC algorithm is briefly derived. Section III is devoted to the derivation of the CSFDE and CSFDEC algorithms, and to the assessment of their computational complexity. The CSFDEC algorithm is then compared, in terms of accuracy and complexity, with other estimation algorithms in Section IV. Finally, some conclusions are offered in Section V.

Notation: Throughout this paper, $(\cdot)^T$ denotes matrix transposition, whereas $(\cdot)^*$ and $(\cdot)^H$ denote complex conjugate and complex conjugate transpose (Hermitian operator), respectively. Moreover, $\Re\{x\}$ and $\Im\{x\}$ indicate the real and imaginary part, respectively, of the complex variable x.

II. System and Signal Models

This section focuses on the processing accomplished at the receive side of a SISO OFDM-based JCAS system; our main objectives are deriving the mathematical model of the received signal in the presence of multiple targets and illustrating some essential assumptions on which it relies. In the following, we take into consideration the transmission of a single frame, consisting of M consecutive OFDM symbols; such symbols can convey both pilot tones (for channel estimation and synchronization) and information data to be sent to a single or multiple receivers at different locations. However, what is relevant in our study is that the considered frame is sent over a wireless channel by a transmitter which is *colocated* with the considered receiver; consequently, the receiver has a full knowledge of the structure and content of the whole frame and of the transmission frequency, and exploits these information for sensing purposes only. The complex envelope of the transmitted signal conveying the mth OFDM symbol (with $m = 0, 1, \ldots, M-1$) of the considered frame can be expressed as (e.g., see [11, eq. (3)])

$$\begin{aligned} x_m(t) &\triangleq x(t - mT_s) \\ &= q(t - mT_s) \sum_{n=0}^{N-1} s_m(n) \exp\left(j2\pi n \Delta_f (t - mT_s)\right), \end{aligned} \tag{1}$$

where $q(t)$ is a windowing function, $s_m(n)$ is the channel symbol carried by the nth subcarrier of the mth OFDM symbol (with $n = 0, 1, \ldots, N-1$), N is the overall number of subcarriers, $\Delta_f = 1/T$ is the subcarrier spacing, T is the OFDM symbol interval, $T_s \triangleq T + T_G$ is the overall duration of the OFDM symbol and T_G is the *cyclic prefix* duration (also known as *guard time* [4]). Following [11], a rectangular windowing function is assumed in this manuscript, so that $q(t) = 1$ for $t \in [-T_G, T]$ and $q(t) = 0$ elsewhere.

Given the complex envelope (1), the *radio frequency* (RF) waveform radiated by the radar transmitter can be expressed as

$$x_{\mathrm{RF}}(t) = \Re\{\exp(j2\pi f_c t) \sum_{m=0}^{M-1} x_m(t)\}, \tag{2}$$

where f_c denotes the frequency of the local oscillator employed in the up-conversion at the transmit side. Let assume

now that the last waveform is reflected by a single scatterer (i.e., by a single *point target*), located at the (initial) distance R from the transmitter and moving at the radial velocity[1] v with respect to it. It is not difficult to show that, in this case, the complex envelope of the signal received by the JCAS system (i.e., by the colocated receiver) is (e.g., see [11, eq. (6)])

$$r(t) = \exp\left(-j2\pi f_{\mathrm{c}}\tau\right)\exp\left(j2\pi f_D t\right) \cdot \sum_{m=0}^{M-1} x\left(t - mT_s - \tau + \frac{f_D}{f_{\mathrm{c}}}t\right) + w\left(t\right), \quad (3)$$

where $\tau \triangleq 2R/c$ is the overall propagation delay, $f_D = 2v/\lambda$ is the Doppler shift due to target motion, $\lambda = c/f_{\mathrm{c}}$ is the wavelength of the radiated signal and $w(t)$ is the complex *additive Gaussian noise* (AGN) process affecting $r(t)$.

The signal $r(t)$ (3) undergoes analog-to-digital conversion followed by DFT processing. A simple mathematical model describing the sequence generated by the sampling of $r(t)$ can be derived as follows. Substituting the *right-hand side* (RHS) of (1) in that of (3) and extracting the portion associated with the mth OFDM symbol from the resulting expression yields

$$r_m(t') = A(\tau)\exp(j2\pi f_D t')\exp(j2\pi f_D m T_s)\sum_{n=0}^{N-1} s_m\left(n\right) \cdot \gamma_n\left(\tau\right)\,\xi_n\left(f_D, t'\right)\cdot\zeta_{m,n}\left(f_D\right)\exp\left(j2\pi n\Delta_f\, t'\right) + w\left(t'\right), \quad (4)$$

where $t' \triangleq t - mT_s$, $A(\tau) \triangleq \exp(-j2\pi f_{\mathrm{c}}\tau)$, $\gamma_n(\tau) \triangleq \exp(-j2\pi n\Delta_f\tau)$, $\xi_n(f_D, t') \triangleq \exp(j2\pi\, n\Delta_f(f_D/f_{\mathrm{c}})t')$ and $\zeta_{m,n}(f_D) \triangleq \exp(j2\pi n\Delta_f(f_D/f_{\mathrm{c}})\, mT_s)$. Note that: 1) the phase of $A(\tau)$ depends on the target delay τ only, whereas that of $\gamma_n(\tau)$ is proportional to both τ and the subcarrier index n; 2) the factor $\xi_n(f_D, t')$ produces a time-dependent phase rotation influenced by both the target speed v and the subcarrier index n; 3) the factor $\zeta_{m,n}(f_D)$ generates a phase rotation depending on both the OFDM symbol index m and the subcarrier index n, and accounts for the so called *intersubcarrier Doppler effect* (e.g., see [11, Sec. II, p. 3]).

Based on (4), it is not difficult to show that, if $|f_D\tau| \ll 1$, sampling $r_m(t')$ (4) at the instant $t'_{m,l} = \tau + T(l/N)$ yields

$$r_m\left(l\right) \triangleq r_m\left(t'_{m,l}\right) = A\left(\tau\right)\exp\left(j2\pi\frac{l}{N}\frac{f_D}{\Delta_f}\right)\exp\left(j2\pi f_D m T_s\right)\sum_{n=0}^{N-1} s_m\left(n\right) \cdot \gamma_n\left(\tau\right)\xi_{n,l}\left(f_D\right)\zeta_{m,n}\left(f_D\right)\exp\left(j2\pi n\frac{l}{N}\right) + w_m\left(l\right), \quad (5)$$

with $l = 0, 1, \ldots, N-1$; here, $\xi_{n,l}(f_D) \triangleq \xi_n(f_D, T\,l/N)$ and $w_m(l) \triangleq w(t'_{m,l})$ is the Gaussian noise affecting $r_m(l)$. In the following, we also assume that: a) the sequence $\{w_m(l); l = 0, 1, \ldots, N-1\}$ can be modelled as *additive white Gaussian noise* (AWGN); b) the target speed is limited, so that $|2v/c| \ll 1/(MN)$ and $|f_D|/\Delta_f = |f_D T| \ll 1$. Consequently, the factors $\exp(j2\pi(lf_D)/(N\Delta_f))$, $\xi_{n,l}(f_D)$, $\zeta_{m,n}(f_D)$ appearing in the RHS of (5) can be neglected; this leads to the simplified signal model

$$r_m(l) = A\left(\tau\right)\exp\left(j2\pi f_D m T_s\right) \cdot \sum_{n=0}^{N-1} s_m(n)\,\gamma_n\left(\tau\right)\exp\left(j2\pi n\frac{l}{N}\right) + w_m\left(l\right), \quad (6)$$

that represents our reference model in the derivation of the CSFDE and CSFDEC algorithms.

The N signal samples acquired in the mth OFDM symbol interval are collected in the vector $\mathbf{r}_m \triangleq [r_m(0), r_m(1), \ldots, r_m(N-1)]^T$, that undergoes order N DFT processing. The nth element of the resulting DFT output vector $\mathbf{R}_m \triangleq [R_m(0), R_m(1), \ldots, R_m(N-1)]^T$ is

$$R_m\left(n\right) \triangleq \frac{1}{N}\sum_{l=0}^{N-1} r_m\left(l\right)\exp\left(-j2\pi\frac{nl}{N}\right) = A\left(\tau\right) \cdot\exp\left(j2\pi f_D m T_s\right)s_m\left(n\right)\exp\left(-j2\pi n\Delta_f\tau\right) + W_m\left(n\right), \quad (7)$$

where $W_m(n)$ is the AWGN sample affecting the nth subcarrier of mth OFDM symbol. Since the channel symbol $s_m(n)$ is known by the JCAS receiver for any n and m, the estimate

$$\hat{H}_{m,n} \triangleq \frac{R_m\left(n\right)}{s_m(n)} = A\left(\tau\right)\, a_m\left(F_D\right)\, a_n\left(-F_r\right) + \bar{W}_m\left(n\right) \quad (8)$$

of the channel frequency response $H_{m,n}$ at the nth subcarrier frequency in the mth OFDM symbol interval can be computed; here, $F_r \triangleq \Delta_f\,\tau$ is the *normalized target delay*, $F_D \triangleq f_D T_s$ is the *normalized Doppler frequency*,[2] $a_q(F_X) \triangleq \exp(j2\pi q F_X)$ (with $q = m$ or n and $X = D$ or r) and

$$\bar{W}_m\left(n\right) \triangleq W_m\left(n\right)/s_m(n) \quad (9)$$

is the noise sample affecting $\hat{H}_{m,n}$ (8). It is worth pointing out that: 1) the parameter F_r (F_D) satisfies the inequalities $F_{r,\min} \leqslant F_r \leqslant F_{r,\max}$, ($F_{D,\min} \leqslant F_D \leqslant F_{D,\max}$), with $F_{r,\min} = 0$ and $F_{r,\max} = 1$ ($F_{D,\min} = -1/2$ and $F_{D,\max} = 1/2$); 2) in all our computer simulations, the channel symbols $\{s_m(n)\}$ belong to a N_s-ary *phase shift keying* (PSK) constellation; 3) based on the last assumption, the noise samples $\{\bar{W}_m(n)\}$ (see (9)) can be modelled as AWGN (the variance of each of them is denoted $\sigma^2_{\bar{W}}$); 4) without any loss of generality, the factor $A(\tau)$ appearing in the RHS of (8) can be replaced by the complex gain $A \triangleq a\exp(j\phi)$, accounting for the phase rotation due to τ, the path loss and the gain (attenuation) introduced by the target.

The model (8) has been derived for a single target, but can be easily generalised to the case of K point targets. In fact, in the last case, (7) becomes

$$R_m\left(n\right) = s_m\left(n\right)\sum_{k=0}^{K-1} A_k\, a_m\left(F_{D_k}\right)\, a_n\left(-F_{r_k}\right) + W_m\left(n\right), \quad (10)$$

[1]This velocity is positive (negative) if the target approaches (moves away from) the considered radar system.

[2]Note that F_r is always a positive quantity, whereas F_D is positive (negative) if the considered target is approaching (moving away from) the radar.

so that $\hat{H}_{m,n}$ (8) can be expressed as

$$\hat{H}_{m,n} = \sum_{k=0}^{K-1} A_k \, a_m \left(F_{D_k}\right) \, a_n \left(-F_{r_k}\right) + \bar{W}_m \left(n\right), \quad (11)$$

with $m = 0, 1, \ldots, M-1$ and $n = 0, 1, \ldots, N-1$; in the last two formulas, F_{r_k}, F_{D_k} and A_k denote the normalized delay, the normalized Doppler frequency and the complex gain, respectively, characterizing the kth target. In the following, we assume that these complex exponentials are ordered according to a decreasing strength, so that $|A_k| \geq |A_{k+1}|$, with $k = 0, \ldots, K-1$.

From (11) it can be easily inferred that: 1) the noisy samples $\{\hat{H}_{m,n}\}$ of the 2D channel response acquired over a single frame can be modelled as the superposition of multiple 2D complex exponentials with AWGN; 2) target detection and estimation is tantamount to identifying the K complex exponentials forming the useful component of the sequence $\{\hat{H}_{m,n}\}$ and estimating their parameters. Finally, it is important to point out that the two normalized frequencies characterizing each target need to be estimated jointly; in fact, if a 1D frequency estimator is used to estimate each of them separately, a complicated pairing problem has to be solved in order to avoid any ambiguity in target detection.

III. Approximate Maximum Likelihood Estimation of Two-Dimensional Complex Tones

In this section, we first derive a novel algorithm for jointly estimating the parameters of a *single* 2D complex tone. Then, we show how this algorithm can be exploited to detect *multiple* superimposed tones and estimate their parameters through a procedure based on successive cancellations and refinements. Finally, we analyse the computational complexity of the developed algorithms, and discuss the similarities and differences of our multiple tone estimator with other related estimation techniques.

A. Joint Estimation of the Parameters of a Single Two-Dimensional Complex Tone

Let us focus on the problem of estimating the parameters of a single 2D complex tone affected by AWGN on the basis of the noisy observations $\{\hat{H}_{m,n}\}$, where (see (8) or, equivalently, (11) with $K = 1$)

$$\hat{H}_{m,n} = A \exp\left(j2\pi m F_D\right) \exp\left(-j2\pi n F_r\right) + \bar{W}_m\left(n\right), \quad (12)$$

with $m = 0, 1, \ldots, M-1$ and $n = 0, 1, \ldots, N-1$. It is easy to show that the ML estimates $F_{D,\mathrm{ML}}$, $F_{r,\mathrm{ML}}$ and A_{ML} of F_D, F_r and A, respectively, can be evaluated as

$$\left(F_{D,\mathrm{ML}}, F_{r,\mathrm{ML}}, A_{\mathrm{ML}}\right) \triangleq \arg \min_{\tilde{F}_D, \tilde{F}_r, \tilde{A}} \varepsilon\left(\tilde{F}_D, \tilde{F}_r, \tilde{A}\right), \quad (13)$$

where $\tilde{F}_D$, $\tilde{F}_r$ and $\tilde{A}$ are the trial values of F_D, F_r and A, respectively,

$$\varepsilon\left(\tilde{F}_D, \tilde{F}_r, \tilde{A}\right) \triangleq \frac{1}{M}\frac{1}{N} \sum_{m=0}^{M-1} \sum_{n=0}^{N-1} \varepsilon_{m,n}\left(\tilde{F}_D, \tilde{F}_r, \tilde{A}\right) \quad (14)$$

is the *mean square error*[3] (MSE) computed over the whole set $\{\hat{H}_{m,n}\}$,

$$\varepsilon_{m,n}\left(\tilde{F}_D, \tilde{F}_r, \tilde{A}\right) \triangleq \left|\hat{H}_{m,n} - H_{m,n}\left(\tilde{F}_D, \tilde{F}_r, \tilde{A}\right)\right|^2 \quad (15)$$

is the *square error* between the noisy sample $\hat{H}_{m,n}$ (12) and its useful component

$$H_{m,n}\left(\tilde{F}_D, \tilde{F}_r, \tilde{A}\right) \triangleq \tilde{A} \exp\left(j2\pi m \tilde{F}_D\right) \exp(-j2\pi n \tilde{F}_r) \quad (16)$$

evaluated under the assumption that $F_D = \tilde{F}_D$, $F_r = \tilde{F}_r$ and $A = \tilde{A}$. Substituting the RHS of the last equation in that of (15) yields

$$\varepsilon_{m,n}\left(\tilde{F}_D, \tilde{F}_r, \tilde{A}\right) = \left|\hat{H}_{m,n}\right|^2 + \left|\tilde{A}\right|^2 - 2\Re\left\{\hat{H}_{m,n} \, \tilde{A}^* \exp\left(-j\left(\tilde{\varphi}_m - \tilde{\phi}_n\right)\right)\right\}, \quad (17)$$

where $\tilde{\varphi}_m \triangleq 2\pi m \tilde{F}_D$ and $\tilde{\phi}_n \triangleq 2\pi n \tilde{F}_r$. Then, substituting the RHS of (17) in that of (14) gives, after some manipulation,

$$\varepsilon\left(\tilde{F}_D, \tilde{F}_r, \tilde{A}\right) = \varepsilon_H + \left|\tilde{A}\right|^2 - 2\Re\left\{\tilde{A}^* \bar{Y}\left(\tilde{F}_D, \tilde{F}_r\right)\right\}, \quad (18)$$

where $\varepsilon_H \triangleq \sum_{m=0}^{M-1} \sum_{n=0}^{N-1} |\hat{H}_{m,n}|^2/(MN)$ and

$$\bar{Y}\left(\tilde{F}_D, \tilde{F}_r\right) \triangleq \frac{1}{MN}\mathrm{SFT}\left[\hat{H}_{m,n}\right] \triangleq \frac{1}{MN} \sum_{m=0}^{M-1} \sum_{n=0}^{N-1} \hat{H}_{m,n} \exp\left(j2\pi n \tilde{F}_r\right) \cdot \exp\left(-j2\pi m \tilde{F}_D\right) \quad (19)$$

is, up to a scale factor, the so called *symplectic Fourier transform* (SFT) of the sequence $\{\hat{H}_{m,n}\}$. It is important out that:

1) The metric $\varepsilon(\tilde{F}_D, \tilde{F}_r, \tilde{A})$ is really optimal in the ML sense, if a PSK constellation is adopted for the channel symbols $\{s_m(n)\}$, so that, as already pointed out in the previous section, an AWGN model can be adopted for the noise sequence $\{\bar{W}_m(n)\}$ (see (12)). On the contrary, if a QAM constellation is selected, the samples of that sequence are not identically distributed, having, in general, different variances (e.g., see [14]); consequently, in the last case, the ML metric can still be put in a form similar to that expressed by (14), but its terms $\{\varepsilon_{m,n}(\tilde{F}_D, \tilde{F}_r, \tilde{A})\}$ cannot be uniformly weighted, being affected by different noise levels.

2) From (18) it is easily inferred that the optimization problem (13) does not admit a closed form solution because of the nonlinear dependence of the metric $\varepsilon(\tilde{F}_D, \tilde{F}_r, \tilde{A})$ (18) on $\tilde{F}_D$ and $\tilde{F}_r$.

The approach we pursued in developing an approximate (but accurate) solution to (13) is based on:

a) Expressing the dependence of the function $\varepsilon(\tilde{F}_D, \tilde{F}_r, \tilde{A})$ on the variables $\tilde{F}_D$ and $\tilde{F}_r$ through the couples $(F_{D,c}, \tilde{\delta}_D)$ and $(F_{r,c}, \tilde{\delta}_r)$ such that

$$\tilde{F}_D = F_{D,c} + \tilde{\delta}_D \, \bar{F}_D \quad (20)$$

[3]It is not difficult to show that, if an arbitrary constellation is selected for the transmitted channel symbols, the optimal metric to be adopted in (13) can be still put in a form similar to (14), the only difference being represented by the fact that $\varepsilon_{m,n}(\tilde{F}_D, \tilde{F}_r, \tilde{A})$ is multiplied by $|s_m(n)|^2$.

and

$$\tilde{F}_r = F_{r,c} + \tilde{\delta}_r \, \bar{F}_r. \tag{21}$$

Here, $F_{D,c}$ ($F_{r,c}$) represents a *coarse estimate* of F_D (F_r), $\tilde{\delta}_D$ and $\tilde{\delta}_r$ are real variables called *residuals*.[4] Moreover, $\bar{F}_D \triangleq 1/M_0$ and $\bar{F}_r \triangleq 1/N_0$ are the *normalized fundamental Doppler frequency* and the *normalized fundamental delay*, respectively, characterizing the order (M_0, N_0) *discrete* SFT (DSFT)

$$\bar{\mathbf{Y}}_{0,0} \triangleq \left[\bar{Y}_{0,0}\,[l,p]\right] \tag{22}$$

of the zero padded version[5]

$$\hat{\mathbf{H}}_{0,0}^{(\mathrm{ZP})} \triangleq \begin{bmatrix} \hat{\mathbf{H}}_{0,0} & \mathbf{0}_{M,N_0-N} \\ \mathbf{0}_{M_0-M,N} & \mathbf{0}_{M_0-M,N_0-N} \end{bmatrix} \tag{23}$$

of the $M \times N$ matrix $\hat{\mathbf{H}}_{0,0} \triangleq [\hat{H}_{m,n}]$ collecting all the elements of the sequence $\{\hat{H}_{m,n}\}$; moreover, in the last equation, $\mathbf{0}_{D_1,D_2}$ is the $D_1 \times D_2$ null matrix, L_D and L_r are positive integers (dubbed *oversampling factors*),

$$M_0 \triangleq L_D \, M \tag{24}$$

and

$$N_0 \triangleq L_r \, N. \tag{25}$$

Note that the element (l,p) of $\bar{\mathbf{Y}}_{0,0}$ (22) is defined as

$$\bar{Y}_{0,0}\,[l,p] \triangleq \frac{1}{M_0 N_0} \sum_{m=0}^{M-1} \sum_{n=0}^{N-1} \hat{H}_{m,n} \, \exp\left(j2\pi np\bar{F}_r\right) \cdot \exp\left(-j2\pi ml\bar{F}_D\right), \tag{26}$$

with $l = 0, 1, \ldots, M_0 - 1$ and $p = 0, 1, \ldots, N_0 - 1$.

b) Assuming that the residuals $\tilde{\delta}_D$ and $\tilde{\delta}_r$ (appearing in the RHS of (20) and (21), respectively) are small, so that Taylor series

$$\exp\left(j\tilde{X}\right) = \sum_{k=0}^{\infty} \frac{j^k \tilde{X}^k}{k!}, \tag{27}$$

truncated to its first four terms (i.e., to the terms associated with $k = 0, 1, 2$ and 3) can be employed to accurately approximate the dependence of the function $\varepsilon(\tilde{F}_D, \tilde{F}_r, \tilde{A})$ on these variables.

c) Exploiting an iterative method, known as *alternating minimization* (AM; e.g., see [16]) to minimise the approximate expression derived for $\varepsilon(\tilde{F}_D, \tilde{F}_r, \tilde{A})$; this allows us to transform the *three-dimensional* (3D) optimization (13) into a triplet of interconnected *one-dimensional* (1D) problems, each referring to a single parameter and, consequently, much easier to be solved than the original ML problem.

Let us show now how these principles can be put into practice. First of all, the exploitation of AM requires solving the following three sub-problems: **P1**) minimizing $\varepsilon(\tilde{F}_D, \tilde{F}_r, \tilde{A})$ with respect to $\tilde{A}$, given $\tilde{F}_D = \hat{F}_D$ and $\tilde{F}_r = \hat{F}_r$; **P2**) minimizing $\varepsilon(\tilde{F}_D, \tilde{F}_r, \tilde{A})$ with respect to $\tilde{F}_D$, given $\tilde{A} = \hat{A}$ and $\tilde{F}_r = \hat{F}_r$; **P3**) minimizing $\varepsilon(\tilde{F}_D, \tilde{F}_r, \tilde{A})$ with respect to $\tilde{F}_r$, given $\tilde{A} = \hat{A}$ and $\tilde{F}_D = \hat{F}_D$. The first sub-problem can be solved exactly thanks to the polynomial dependence of the cost function $\varepsilon(\tilde{F}_D, \tilde{F}_r, \tilde{A})$ (18) on the variable $\tilde{A}$. In fact, the function $\varepsilon(\hat{F}_D, \hat{F}_r, \tilde{A})$ is minimized with respect to $\tilde{A}$ if[6]

$$\tilde{A} = \hat{A} = \bar{Y}\left(\hat{F}_D, \hat{F}_r\right), \tag{28}$$

where $\bar{Y}(\hat{F}_D, \hat{F}_r)$ can be computed exactly through its expression (19) or, in an approximate fashion, through a computationally efficient procedure based on the fact that the matrix

$$\bar{\mathbf{Y}}_s \triangleq L_D \, L_r \, \bar{\mathbf{Y}}_{0,0} \tag{29}$$

collects $M_0 \times N_0$ uniformly spaced samples of the function $\bar{Y}(\tilde{F}_D, \tilde{F}_r)$, since $\bar{Y}_{0,0}[l,p] = \bar{Y}(l\bar{F}_D, \, p\bar{F}_r)/(L_D \, L_r)$ (see (19), (24)-(26)). For this reason, if one of the normalized frequencies $\hat{F}_D$ and $\hat{F}_r$ or both of them are not a multiple of $\bar{F}_D$ and $\bar{F}_r$, respectively, an approximate evaluation of $\bar{Y}(\hat{F}_D, \hat{F}_r)$ can be accomplished by *interpolating*[7] the elements of the matrix $\bar{\mathbf{Y}}_s$ (29). Note also that the last matrix can be efficiently computed by performing an order N_0 *inverse fast Fourier transform* (IFFT) along the rows of $\hat{\mathbf{H}}_{0,0}^{(\mathrm{ZP})}$ (23), followed an order M_0 *fast Fourier transform* (FFT) along the columns of the resulting matrix.

Let us take into consideration now **P2** and **P3**. Such sub-problems, unlike the previous one, do not admit closed form solutions. However, approximate solutions can be developed by: 1) representing the parameters F_D and F_r in the same form as $\tilde{F}_D$ (20) and $\tilde{F}_r$ (21), respectively, i.e. as $F_D = F_{D,c} + \delta_D \, \bar{F}_D$ and $F_r = F_{r,c} + \delta_r \, \bar{F}_r$, respectively; 2) using the 2D *periodogram method* to estimate $F_{D,c}$ and $F_{r,c}$; 3) devising a novel algorithm for estimating the residuals δ_D and δ_r, i.e. for accomplishing the *fine estimation* of F_D and F_r, respectively. The fine estimation algorithm is derived as follows. Based on the representations (20) and (21) of the trial variables $\tilde{F}_D$ and $\tilde{F}_r$, respectively, the variables $\tilde{\varphi}_m$ and $\tilde{\phi}_n$ defined right after (17) are expressed as $\tilde{\varphi}_m = 2\pi m \, F_{D,c} + m\tilde{\Omega}$ and $\tilde{\phi}_n = 2\pi n \, F_{r,c} + n\tilde{\Delta}$, respectively; here, $\tilde{\Omega} \triangleq 2\pi\tilde{\delta}_D \, \bar{F}_D$ and $\tilde{\Delta} \triangleq 2\pi\tilde{\delta}_r \, \bar{F}_r$. Then, the following steps are accomplished: 1) the new expressions of $\tilde{\varphi}_m$ and $\tilde{\phi}_n$ are substituted in the RHS of (17); 2) the resulting expression is substituted in the RHS of (14) and the approximation (27) is adopted for $\exp(jm\tilde{\Omega})$ and $\exp(jn\tilde{\Delta})$ under the assumption that both $\tilde{\Omega}$ and $\tilde{\Delta}$ are small enough.[8] This yields, after some manipulation, the approximate expression

$$\varepsilon_{\mathrm{CSFDE}}\left(\tilde{\Omega}, \tilde{\Delta}, \hat{A}\right) \triangleq \varepsilon_H + \left|\hat{A}\right|^2 - 2\xi\left(\tilde{\Omega}, \tilde{\Delta}, \hat{A}\right) \tag{30}$$

[4]The decomposition of an unknown frequency into the sum of a multiple of a given *fundamental frequency* and a *frequency residual* is commonly adopted in the technical literature concerning ML frequency estimation (e.g., see [15] and references therein).

[5]Note that the following definition represents a specific case of the matrix $\hat{\mathbf{H}}_{k_1,k_2}^{(\mathrm{ZP})}$ defined right after (33) (in particular, its corresponds to the choice $k_1 = k_2 = 0$).

[6]This represents a straightforward generalisation of a mathematical result which is well known in 1D ML frequency estimation (e.g., see [17, Sec. IV]).

[7]See [18] for *polynomial interpolation* and [19] for *barycentric interpolation*.

[8]This is equivalent to assuming that $1/M_0$ and $1/N_0$ are small enough (i.e., that M_0 and N_0 are large enough).

for the function $\varepsilon(\tilde{F}_D, \tilde{F}_r, \tilde{A})$ (14); here,

$$\xi\left(\tilde{\Omega}, \tilde{\Delta}, \hat{A}\right) = \sum_{p=0}^{3}\sum_{q=0}^{3} (-1)^{(p+q)} \frac{\tilde{\Omega}^p \tilde{\Delta}^q}{p!q!} \Re\left\{ j^{(p-q)} \hat{A}^* \bar{Y}_{p,q} \right\}, \tag{31}$$

$$\bar{Y}_{k_1,k_2}(\rho_D, \rho_r) \triangleq \frac{1}{MN} \sum_{m=0}^{M-1}\sum_{n=0}^{N-1} \hat{H}_{m,n}^{(k_1,k_2)} \exp\left(j\frac{2\pi n \rho_r}{N_0}\right) \cdot \exp\left(-j\frac{2\pi m \rho_D}{M_0}\right), \tag{32}$$

$\rho_D \triangleq F_{D,c}/\bar{F}_D$, $\rho_r \triangleq F_{r,c}/\bar{F}_r$ and $\hat{H}_{m,n}^{(k_1,k_2)} \triangleq m^{k_1} n^{k_2} \hat{H}_{m,n}$, with $m = 0, 1, \ldots, M-1$ and $n = 0, 1, \ldots, N-1$. It is important to point out that: a) if both ρ_D and ρ_r are integers, the quantity $\bar{Y}_{k_1,k_2}(\rho_D, \rho_r)$ (32) represents the element (ρ_D, ρ_r) of the $M_0 \times N_0$ matrix

$$\bar{\mathbf{Y}}_{k_1,k_2} \triangleq \mathrm{DSFT}\left[\hat{\mathbf{H}}_{k_1,k_2}^{(\mathrm{ZP})}\right] \tag{33}$$

generated by the order (M_0, N_0) DSFT of the zero padded version of the $M \times N$ matrix[9] $\hat{\mathbf{H}}_{k_1,k_2} \triangleq [\hat{H}_{m,n}^{(k_1,k_2)}]$; b) if the previous condition is not met, the quantity $\bar{Y}_{k_1,k_2}(\rho_D, \rho_r)$ can be evaluated exactly on the basis of (32) or, in an approximate fashion, by interpolating multiple adjacent elements of the matrix $L_D\, L_r\, \bar{\mathbf{Y}}_{k_1,k_2}$ (see (33)).

Minimizing $\varepsilon_{\mathrm{CSFDE}}(\tilde{\Omega}, \tilde{\Delta}, \hat{A})$ (30) is equivalent to maximizing the function $\xi(\tilde{\Omega}, \tilde{\Delta}, \hat{A})$ (31). The last function can be easily maximized with respect to the variable $\tilde{\Omega}$ ($\tilde{\Delta}$) if $\tilde{\Delta}$ ($\tilde{\Omega}$) is known. Therefore, given $\tilde{\Delta} = \hat{\Delta}$, the estimate $\hat{\delta}_D \triangleq \hat{\Omega}/(2\pi\bar{F}_D)$ of δ_D can be evaluated by taking the derivative of $\xi(\tilde{\Omega}, \hat{\Delta}, \hat{A})$ with respect to $\tilde{\Omega}$ and setting it to zero. In fact, this leads to the estimate[10]

$$\hat{X} = \frac{-b_X + \sqrt{b_X^2 - 4\, a_X\, c_X}}{2\, a_X}, \tag{34}$$

that represents one of the two solutions of the quadratic equation

$$a_X\, \tilde{X}^2 + b_X\, \tilde{X} + c_X = 0, \tag{35}$$

with $X = \Omega$; here,

$$a_\Omega = -\hat{\Delta}^3\, \Re\left\{\hat{A}^* \bar{Y}_{3,3}\right\}/6 - \hat{\Delta}^2\, \Im\left\{\hat{A}^* \bar{Y}_{3,2}\right\}/2 + \hat{\Delta}\, \Re\left\{\hat{A}^* \bar{Y}_{3,1}\right\} + \Im\left\{\hat{A}^* \bar{Y}_{3,0}\right\}, \tag{36}$$

$$b_\Omega = \hat{\Delta}^3\, \Im\left\{\hat{A}^* \bar{Y}_{2,3}\right\}/3 - \hat{\Delta}^2\, \Re\left\{\hat{A}^* \bar{Y}_{2,2}\right\} - 2\hat{\Delta}\, \Im\left\{\hat{A}^* \bar{Y}_{2,1}\right\} + 2\Re\left\{\hat{A}^* \bar{Y}_{2,0}\right\}, \tag{37}$$

$$c_\Omega = \hat{\Delta}^3\, \Re\left\{\hat{A}^* \bar{Y}_{1,3}\right\}/3 + \hat{\Delta}^2\, \Im\left\{\hat{A}^* \bar{Y}_{1,2}\right\} - 2\hat{\Delta}\, \Re\left\{\hat{A}^* \bar{Y}_{1,1}\right\} - 2\Im\left\{\hat{A}^* \bar{Y}_{1,0}\right\}. \tag{38}$$

A simpler estimate (denoted $\hat{\Omega}'$) of Ω is obtained neglecting the contribution of the quadratic term in the *left-hand side* (LHS) of (35), i.e. setting $a_\Omega = 0$. This leads to a first-degree equation, whose solution is (with $X = \Omega$)

$$\hat{X}' = -c_X/b_X. \tag{39}$$

Dually, given $\tilde{\Omega} = \hat{\Omega}$, an estimate $\hat{\delta}_r \triangleq \hat{\Delta}/(2\pi\bar{F}_r)$ of $\tilde{\delta}_r$ is computed by taking the derivative of $\xi(\hat{\Omega}, \tilde{\Delta}, \hat{A})$ with respect to $\tilde{\Delta}$ and setting it to zero. This leads to a quadratic equation in the variable $\tilde{\Delta}$ whose structure is still expressed by (35) (with $X = \Delta$); however, its coefficients are

$$a_\Delta = -\hat{\Omega}^3\, \Re\left\{\hat{A}^* \bar{Y}_{3,3}\right\}/6 + \hat{\Omega}^2\, \Im\left\{\hat{A}^* \bar{Y}_{2,3}\right\}/2 + \hat{\Omega}\, \Re\left\{\hat{A}^* \bar{Y}_{1,3}\right\} - \Im\left\{\hat{A}^* \bar{Y}_{0,3}\right\}, \tag{40}$$

$$b_\Delta = -\hat{\Omega}^3\, \Im\left\{\hat{A}^* \bar{Y}_{3,2}\right\}/3 - \hat{\Omega}^2\, \Re\left\{\hat{A}^* \bar{Y}_{2,2}\right\} + 2\hat{\Omega}\, \Im\left\{\hat{A}^* \bar{Y}_{1,2}\right\} + 2\Re\left\{\hat{A}^* \bar{Y}_{0,2}\right\}, \tag{41}$$

$$c_\Delta = \hat{\Omega}^3\, \Re\left\{\hat{A}^* \bar{Y}_{3,1}\right\}/3 - \hat{\Omega}^2\, \Im\left\{\hat{A}^* \bar{Y}_{2,1}\right\} - 2\hat{\Omega}\, \Re\left\{\hat{A}^* \bar{Y}_{1,1}\right\} + 2\Im\left\{\hat{A}^* \bar{Y}_{0,1}\right\}. \tag{42}$$

For this reason, the estimates $\hat{\Delta}$ and $\hat{\Delta}'$ of Δ can be computed on the basis of (34) and (39), respectively.

Given the estimate $\hat{\delta}_D$ ($\hat{\delta}_r$) of δ_D (δ_r), a *fine estimate* $\hat{F}_D$ of F_D ($\hat{F}_r$ of F_r) can be evaluated on the basis of (20) ((21)).

The previous mathematical results allow us to easily develop an AM-based procedure for estimating the parameters F_D, F_r and A in an iterative fashion. This procedure, dubbed CSFDE, is initialized by computing: 1) the $M_0 \times N_0$ matrices[11] $\{\bar{\mathbf{Y}}_{k_1,k_2}; k_1, k_2 = 0, 1, 2, 3\}$ (see (33)); 2) the coarse estimates $\hat{F}_{D,c}^{(0)} = \hat{l}\,\bar{F}_D - 1/2$ and $\hat{F}_{r,c}^{(0)} = \hat{p}\bar{F}_r$ of F_D and F_r, respectively, where

$$\left(\hat{l}, \hat{p}\right) = \arg \max_{\tilde{l} \in \mathcal{S}_{M_0}, \tilde{p} \in \mathcal{S}_{N_0}} \left\| \bar{Y}_{0,0}\left[\tilde{l}, \tilde{p}\right] \right\|^2 \tag{43}$$

and $\mathcal{S}_X \triangleq \{0, 1, \ldots, X-1\}$ for any positive integer X; 3) the initial estimate $\hat{A}^{(0)}$ of $\tilde{A}$ on the basis of (28), with $(\hat{F}_D, \hat{F}_r) = (\hat{F}_{D,c}^{(0)}, \hat{F}_{r,c}^{(0)})$; 4) the coefficients $\{a_\Omega, b_\Omega, c_\Omega\}$ ($\{a_\Delta, b_\Delta, c_\Delta\}$) for $(\rho_D, \rho_r) = (\hat{l}^{(0)}, \hat{p}^{(0)})$) according to (37)-(38) ((40)-(42)); 5) the initial estimate $\hat{\Omega}^{(0)}(\hat{\Delta}^{(0)})$ of Ω (Δ) on the basis of (34) or (39) with $X = \Omega$ (with $X = \Delta$); 6) the initial fine estimates (see (20) and (21))

$$\hat{F}_D^{(0)} = \hat{F}_{D,c}^{(0)} + \hat{\Omega}^{(0)}/(2\pi) \tag{44}$$

and

$$\hat{F}_r^{(0)} = \hat{F}_{r,c}^{(0)} + \hat{\Delta}^{(0)}/(2\pi) \tag{45}$$

of F_D and F_r, respectively. Finally, we set the iteration index i to 1 and start an iterative procedure. The ith iteration is fed by the estimates $\hat{F}_D^{(i-1)}$, $\hat{F}_r^{(i-1)}$ and $\hat{A}^{(i-1)}$ of F_D, F_r and A, respectively, and produces the new estimates $\hat{F}_D^{(i)}$, $\hat{F}_r^{(i)}$ and $\hat{A}^{(i)}$ of the same quantities (with $i = 1, 2, \ldots, N_{\mathrm{it}}$, where N_{it} is the overall number of iterations). The procedure adopted for

[9]Note that $\hat{\mathbf{H}}_{k_1,k_2}^{(\mathrm{ZP})}$ has the same structure as $\hat{\mathbf{H}}_{0,0}^{(\mathrm{ZP})}$ (23), the only difference being represented by the fact that, in its definition, $\hat{\mathbf{H}}_{0,0}$ is replaced by $\hat{\mathbf{H}}_{k_1,k_2}$.

[10]In the following equations, the dependence of the function $\bar{Y}_{k_1,k_2}(\rho_D, \rho_r)$ (32) and of the coefficients $\{a_X, b_X, c_X\}$ on (ρ_D, ρ_r) is not explicitly specified to ease reading.

[11]Note that the matrices $\{\bar{\mathbf{Y}}_{k_1,k_2}\}$ corresponding to $(k_1, k_2) = (0, 3)$, $(3, 0)$ and $(3, 3)$ are not required if the simpler estimates $\hat{\Omega}'$ and $\hat{\Delta}'$ are evaluated.

the evaluation of $\hat{F}_D^{(i)}$, $\hat{F}_r^{(i)}$ and $\hat{A}^{(i)}$ consists of the two steps described below.

1) *Estimation of the normalized Doppler and the normalized delay* - The new estimates $\hat{\Omega}^{(i)}$ and $\hat{\Delta}^{(i)}$ of $\tilde{\Omega}$ and $\tilde{\Delta}$, respectively, are computed according to (34) or (39). In the evaluation of the coefficients of these equations, $\hat{A} = \hat{A}^{(i-1)}$,

$$\rho_D = \hat{\rho}_D^{(i-1)} = \hat{F}_D^{(i-1)} / \bar{F}_D \tag{46}$$

and

$$\rho_r = \hat{\rho}_r^{(i-1)} = \hat{F}_r^{(i-1)} / \bar{F}_r \tag{47}$$

are assumed. Then,

$$\hat{F}_D^{(i)} = \hat{F}_D^{(i-1)} + \hat{\Omega}^{(i)} / (2\pi) \tag{48}$$

and

$$\hat{F}_r^{(i)} = \hat{F}_r^{(i-1)} + \hat{\Delta}^{(i)} / (2\pi) \tag{49}$$

are computed.

2) *Estimation of the complex amplitude* - The new estimate $\hat{A}^{(i)}$ of $\hat{A}$ is evaluated by means of (28); in doing so, $\hat{F}_D = \hat{F}_D^{(i)}$ and $\hat{F}_r = \hat{F}_r^{(i)}$ are assumed.

The index i is incremented by one before starting the next iteration. At the end of the last (i.e. of the $N_{\rm it}$th) iteration, the fine estimates $\hat{F}_D = \hat{F}_D^{(N_{\rm it})}$, $\hat{F}_r = \hat{F}_r^{(N_{\rm it})}$ and $\hat{A} = \hat{A}^{(N_{\rm it})}$ of F_D, F_r and A, respectively, become available. The CSFDE algorithm is summarized in Algorithm 1.

It is worth pointing out that: 1) the initial coarse estimates $\hat{F}_{D,c}^{(0)}$ (44) and $\hat{F}_{r,c}^{(0)}$ (45) are computed by resorting to the 2D *periodogram method* (see (43)); 2) unlike traditional DFT-based methods, the CSFDE algorithm requires the evaluation of multiple DSFTs and, more precisely, of 16 (13) DSFTs $\{\bar{\mathbf{Y}}_{k_1,k_2}\}$ if (34) ((39)) is employed in the evaluation of the estimates of Ω and Δ; 3) the approximate ML metric $\varepsilon_{\rm CSFDE}(\tilde{\Omega}, \tilde{\Delta}, \hat{A})$ (30) on which the CSFDE algorithm is based is new; 4) the estimates $\hat{\delta}_D^{(i)}$ ($\hat{\delta}_r^{(i)}$) of δ_D (δ_r) computed by the CSFDE algorithm in its ith iteration are expected to become smaller as i increases, since $\hat{F}_D^{(i)}$ ($\hat{F}_r^{(i)}$) should progressively approach F_D (F_r) if this algorithm converges.

Algorithm 1 Complex Single Frequency-Delay Estimator (CSFDE)

Input: The matrices $\{\mathbf{Y}_{k_1,k_2}; k_1, k_2 = 0, 1, 2 \text{ and } 3\}$ (see (33)) and the value of the parameter $N_{\rm it}$.

Initialization:

a- Evaluate $\bar{\mathbf{Y}}_{0,0}$ (22), $\hat{l}$ and $\hat{p}$ (see (43)); then, compute the initial estimate $\hat{A}^{(0)}$ of A according to (28) and set $(\rho_D^{(0)}, \rho_r^{(0)}) = (\hat{l}, \hat{p})$ (see (46)-(47)).

b- Compute the coefficients a_Ω, b_Ω and c_Ω according to (36)-(38); then, evaluate $\hat{\Omega}^{(0)}$ according to (34) or (39).

c- Evaluate the coefficients a_Δ, b_Δ and c_Δ according to (40)-(42); then, compute $\hat{\Delta}^{(0)}$ according to (34) or (39).

d- Compute $\hat{F}_D^{(0)}$ and $\hat{F}_r^{(0)}$ according to (44) and (45), respectively.

Refinement: for $i = 1$ *to* $N_{\rm it}$ **do**

e- *Estimation of* A: Set $\hat{F}_D = \hat{F}_D^{(i-1)}$ and $\hat{F}_r = \hat{F}_r^{(i-1)}$; then, evaluate $\bar{Y}(\hat{F}_D, \hat{F}_r)$ using (19) or by interpolating a few adjacent elements of the matrix $\bar{\mathbf{Y}}_s$ (29). Finally, compute $\hat{A}^{(i)}$, $\hat{\rho}_D^{(i-1)}$ and $\hat{\rho}_r^{(i-1)}$ according to (28), (46) and (47), respectively.

f- *Estimation of* F_D: Set $\hat{A} = \hat{A}^{(i)}$ and compute $\bar{Y}_{k_1,k_2}(\hat{\rho}_D^{(i-1)}, \hat{\rho}_r^{(i-1)})$ according to (32) or by interpolating a few adjacent elements of $\bar{\mathbf{Y}}_{k_1,k_2}$ (33); then, compute a_Ω, b_Ω and c_Ω according to (36)-(38) assuming $(\rho_D, \rho_r) = (\hat{\rho}_D^{(i-1)}, \hat{\rho}_r^{(i-1)})$. Finally, compute $\hat{\Omega}^{(i)}$ and $\hat{F}_D^{(i)}$ according to (34) (or (39)) and (48), respectively.

g- *Estimation of* F_r: Compute $a_{\tilde{\Delta}}$, $b_{\tilde{\Delta}}$ and $c_{\tilde{\Delta}}$ according to (40)-(42) under the assumption that $(\rho_D, \rho_r) = (\hat{\rho}_D^{(i-1)}, \hat{\rho}_r^{(i-1)})$; then, evaluate $\hat{\Delta}^{(i)}$ and $\hat{F}_r^{(i)}$ on the basis of (34) (or (39)) and (49), respectively.

end

Output: The estimates $\hat{F}_D^{(N_{\rm it})}$, $\hat{F}_r^{(N_{\rm it})}$ and $\hat{A}^{(N_{\rm it})}$ of F_D, F_r and A, respectively.

B. Estimation of Multiple Two-Dimensional Tones

Let us show now how the CSFDE algorithm can be exploited to recursively estimate the multiple tones forming the useful component of the complex sequence $\{\hat{H}_{m,n}\}$, whose (m,n)th element is expressed by (11), where K is assumed to be greater than unity and *unknown*. The method we develop to achieve this objective is called *complex single frequency-delay estimation and cancellation* (CSFDEC) and is based on the idea of 1) separating the contribution of the first (and strongest tone) in the RHS of (11) from that of the remaining $(K-1)$ tones and 2) considering the latter contribution as part of the overall noise affecting the former one. Based on this representation of $\{\hat{H}_{m,n}\}$, an estimate of the parameters (A_0, F_{D_0}, F_{r_0}) can be evaluated through the CSFDE and can be employed to subtract the contribution of the first tone to $\{\hat{H}_{m,n}\}$, so generating a residual measurement. This estimation & cancellation procedure is repeated to recursively estimate the other tones on the basis of the computed residuals until the energy of the last residual falls below a given threshold; this generates, as a by-product, an estimate of K. Moreover, in the CSFDEC method, after detecting a new tone and estimating its parameters, a *re-estimation* technique is executed to improve the accuracy of both this tone and the previously estimated tones.

The CSFDEC algorithm is initialized by: 1) running the CSFDE algorithm to compute the initial estimates $\hat{F}_{D_0}^{(0)}$, $\hat{F}_{r_0}^{(0)}$ and $\hat{A}_0^{(0)}$ of the parameters F_{D_0}, F_{r_0} and A_0 characterizing the first target; 2) setting the recursion index i to 1 and $\bar{\mathbf{Y}}_{0,0}^{(0)} = \bar{\mathbf{Y}}_{0,0}$ (see (22)). Then, a recursive procedure is started. The ith recursion of this procedure is fed by the vectors $\hat{\mathbf{F}}_D^{(i-1)} = [\hat{F}_{D_0}^{(i-1)}, \hat{F}_{D_1}^{(i-1)}, \ldots, \hat{F}_{D_{i-1}}^{(i-1)}]^T$, $\hat{\mathbf{F}}_r^{(i-1)} = [\hat{F}_{r_0}^{(i-1)}, \hat{F}_{r_1}^{(i-1)}, \ldots, \hat{F}_{r_{i-1}}^{(i-1)}]^T$ and $\hat{\mathbf{A}}^{(i-1)} = [\hat{A}_0^{(i-1)}, \hat{A}_1^{(i-1)}, \ldots, \hat{A}_{i-1}^{(i-1)}]^T$, collecting the estimates of the normalized Doppler frequency, normalized delay and complex amplitude, respectively, of the i tones detected and estimated in the previous recursions, and generates the new vectors $\hat{\mathbf{F}}_D^{(i)}$,

$\hat{\mathbf{F}}_r^{(i)}$ and $\hat{\mathbf{A}}^{(i)}$ after: a) estimating the parameters $\hat{F}_{D_i}^{(i)}$, $\hat{F}_{r_i}^{(i)}$ and $\hat{A}_i^{(i)}$ of the new (i.e., of the ith) tone (if any); b) refining the estimates of the i tones available at the beginning of the considered recursion. The procedure employed for accomplishing all this consists of the three steps described below (the p th step is denoted CSFDE-Sp, with $p = 1$, 2 and 3)

CSFDEC-S1 (*spectral cancellation and estimation of a new tone*) - In this step, the following quantities are evaluated (see the initialization part of the CSFDE algorithm):

a) The *residual spectrum*

$$\mathbf{Y}_{0,0}^{(i)} = [\bar{Y}_{0,0}^{(i)}[l,p]] \triangleq \mathbf{Y}_{0,0}^{(i-1)} - \mathbf{C}_{0,0}^{(i)}\big(\hat{\mathbf{A}}^{(i-1)}, \hat{\mathbf{F}}_D^{(i-1)}, \hat{\mathbf{F}}_r^{(i-1)}\big), \quad (50)$$

where

$$\mathbf{C}_{0,0}^{(i)}\big(\hat{\mathbf{A}}^{(i-1)}, \hat{\mathbf{F}}_D^{(i-1)}, \hat{\mathbf{F}}_r^{(i-1)}\big) \triangleq \sum_{k=0}^{i-1} \bar{\mathbf{C}}_{0,0}\big(\hat{A}_k^{(i-1)}, \hat{F}_{D_k}^{(i-1)}, \hat{F}_{r_k}^{(i-1)}\big) \quad (51)$$

represents the contribution given by all the ith estimated 2D tones to $\bar{\mathbf{Y}}_{0,0}$ and $\bar{\mathbf{C}}_{0,0}(\hat{A}_k^{(i-1)}, \hat{F}_{D_k}^{(i-1)}, \hat{F}_{r_k}^{(i-1)})$ is the contribution provided by the kth tone (with $k = 0, 1, \ldots, i-1$) to the same matrix (the expression of the elements of the matrix $\bar{\mathbf{C}}_{0,0}(\cdot,\cdot,\cdot)$ is derived in Appendix A; see (60)). If the overall energy $\varepsilon_{0,0}[i] \triangleq \|\mathbf{Y}_{0,0}^{(i)}\|^2$ of the vector $\mathbf{Y}_{0,0}^{(i)}$ (50) satisfies the inequality $\varepsilon_{0,0}[i] < T_{\mathrm{CSFDEC}}$, where T_{CSFDEC} is a proper threshold, the algorithm stops and the estimate $\hat{K} = i$ of K is generated.

b) The couple of integers $(\hat{l}^{(i)}, \hat{p}^{(i)})$ on the basis of (43) (where, however, $\bar{Y}_{0,0}[\tilde{l},\tilde{p}]$ is replaced by $\bar{Y}_{0,0}^{(i)}[\tilde{l},\tilde{p}]$) and the coarse estimates $\hat{F}_{D,c_i}^{(i)} = \hat{l}^{(i)}\bar{F}_D - 1/2$ and $\hat{F}_{r,c_i}^{(i)} = \hat{p}^{(i)}\bar{F}_r$ of $F_{D,c}$ and $F_{r,c}$, respectively.

c) The preliminary estimate (see (28))

$$\bar{A}_i^{(i)} = \bar{Y}(\hat{F}_{D,c_i}^{(i)}, \hat{F}_{r,c_i}^{(i)}) - \breve{Y}_{0,0}\left(\hat{F}_{D,c_i}^{(i)}, \hat{F}_{r,c_i}^{(i)}; \hat{\mathbf{A}}^{(i-1)}, \hat{\mathbf{F}}_D^{(i-1)}, \hat{\mathbf{F}}_r^{(i-1)}\right) \quad (52)$$

of the complex amplitude A_i; here,

$$\breve{Y}_{0,0}\left(\hat{F}_{D,c_i}^{(i)}, \hat{F}_{r,c_i}^{(i)}; \hat{\mathbf{A}}^{(i-1)}, \hat{\mathbf{F}}_D^{(i-1)}, \hat{\mathbf{F}}_r^{(i-1)}\right) \triangleq \sum_{k=0}^{i-1} \bar{Y}_{0,0}\left(\hat{F}_{D,c_i}^{(i)}, \hat{F}_{r,c_i}^{(i)}; \hat{A}_k^{(i-1)}, \hat{F}_{D_k}^{(i-1)}, \hat{F}_{r_k}^{(i-1)}\right) \quad (53)$$

is the contribution given to $\bar{Y}(\hat{F}_{D,c_i}^{(i)}, \hat{F}_{r,c_i}^{(i)})$ by the first i estimated tones for $(F_D, F_r) = (\hat{F}_{D,c_i}^{(i)}, \hat{F}_{r,c_i}^{(i)})$ and $\bar{Y}_{0,0}(\hat{F}_{D,c_i}^{(i)}, \hat{F}_{r,c_i}^{(i)}; \hat{A}_k^{(i-1)}, \hat{F}_{D_k}^{(i-1)}, \hat{F}_{r_k}^{(i-1)})$ represents the leakage due to the kth tone and affecting the ith tone. The expression of the quantity $\bar{Y}_{k_1,k_2}(\hat{F}_{D,c_i}^{(i)}, \hat{F}_{r,c_i}^{(i)}; \hat{A}_k^{(i-1)}, \hat{F}_{D_k}^{(i-1)}, \hat{F}_{r_k}^{(i-1)})$ is provided in Appendix B (see (63)).

d) The spectral coefficients

$$\bar{Y}_{k_1,k_2}^{(i)}\left(\rho_D^{(i)}, \rho_r^{(i)}\right) = \bar{Y}_{k_1,k_2}\left(\rho_D^{(i)}, \rho_r^{(i)}\right) - \breve{Y}_{k_1,k_2}\left(\hat{F}_{D,c_i}^{(i)}, \hat{F}_{r,c_i}^{(i)}; \hat{\mathbf{A}}^{(i-1)}, \hat{\mathbf{F}}_D^{(i-1)}, \hat{\mathbf{F}}_r^{(i-1)}\right), \quad (54)$$

with $k_1, k_2 = 0, 1, 2, 3$; here, $\rho_D^{(i)} = \hat{F}_{D,c_i}^{(i)}/\bar{F}_D = \hat{l}^{(i)} - 1/(2\bar{F}_D)$ and $\rho_r^{(i)} = \hat{F}_{r,c_i}^{(i)}/\bar{F}_r = \hat{p}^{(i)}$ (see (46) and (47), respectively), whereas

$$\breve{Y}_{k_1,k_2}\left(\hat{F}_{D,c_i}^{(i)}, \hat{F}_{r,c_i}^{(i)}; \hat{\mathbf{A}}^{(i-1)}, \hat{\mathbf{F}}_D^{(i-1)}, \hat{\mathbf{F}}_r^{(i-1)}\right) \triangleq \sum_{k=0}^{i-1} \bar{Y}_{k_1,k_2}\left(\hat{F}_{D,c_i}^{(i)}, \hat{F}_{r,c_i}^{(i)}; \hat{A}_k^{(i-1)}, \hat{F}_{r_k}^{(i-1)}, \hat{F}_{D_k}^{(i-1)}\right) \quad (55)$$

represents the contribution given to $\bar{Y}_{k_1,k_2}^{(i)}(\rho_D^{(i)}, \rho_r^{(i)})$ by all the estimated tones (in particular, the term $\bar{Y}_{k_1,k_2}(\cdot,\cdot;\cdot,\cdot,\cdot)$ appearing in the RHS of (55) represents the leakage due to the k th estimated tone for $(F_D, F_r) = (\hat{F}_{D,c_i}^{(i)}, \hat{F}_{r,c_i}^{(i)})$);

e) The coefficients $\{a_\Omega, b_\Omega, c_\Omega\}$ ($\{a_\Delta, b_\Delta, c_\Delta\}$) on the basis of (36)-(38) ((40)-(42)) with $(\rho_D, \rho_r) = (\rho_D^{(i)}, \rho_r^{(i)})$ and the initial estimate of the residual $\hat{\Omega}_i^{(0)}(\hat{\Delta}_i^{(0)})$ of Ω (Δ) on the basis of (34) or (39) with $X = \Omega$ ($X = \Delta$);

f) The initial fine estimate of the normalized Doppler frequency $\hat{F}_{D_i}^{(0)} = \hat{F}_{D,c_i}^{(0)} + \hat{\Omega}_i^{(0)}/(2\pi)$ and that of the normalized delay $\hat{F}_{r_i}^{(0)} = \hat{F}_{r,c_i}^{(0)} + \hat{\Delta}_i^{(0)}/(2\pi)$ (see (20) and (21), respectively). The evaluation of $\hat{F}_D^{(0)}$ and $\hat{F}_r^{(0)}$ concludes the first step.

CSFDEC-S2 (*refinement of the last tone*) - In this step, N_{it} iterations are executed to refine the estimate of the parameters of the new tone detected in the previous step. The processing accomplished in this step follows closely that described in the refinement part (i.e., in the second step) of the CSFDE. For this reason, in each iteration, new estimates of the complex amplitude and of the two residuals are computed for the ith tone. This requires reusing (52)-(53) and (54)-(55) for the removal of spectral leakage. At the end of the last iteration, the estimates $(\check{F}_{D_i}^{(i)}, \check{F}_{r_i}^{(i)}, \check{A}_i^{(i)})$ of (F_{D_i}, F_{r_i}, A_i) are available; these estimates represent $(\hat{F}_{D_i}^{(i)}, \hat{F}_{r_i}^{(i)}, \hat{A}_i^{(i)})$ if the next step is not accomplished (i.e. if tone re-estimation is avoided).

CSFDEC-S3 (*tone re-estimation*) - This step is fed by the $(i+1)$ normalized delays $\{\hat{F}_{r_0}^{(i-1)}, \hat{F}_{r_1}^{(i-1)}, \ldots, \hat{F}_{r_{i-1}}^{(i-1)}, \check{F}_{r_i}^{(i)}\}$, the normalized Doppler frequencies $\{\hat{F}_{D_0}^{(i-1)}, \hat{F}_{D_1}^{(i-1)}, \ldots, \hat{F}_{D_{i-1}}^{(i-1)}, \check{F}_{r_i}^{(i)}\}$ and the associated complex amplitudes $\{\hat{A}_0^{(i-1)}, \hat{A}_1^{(i-1)}, \ldots, \hat{A}_{i-1}^{(i-1)}, \check{A}_i^{(i)}\}$. It consists in repeating the previous step for each of the detected tones, starting from the first tone and ending with the last (i.e., with the $(i+1)$th) one. This means that, when re-estimating the kth tone, the leakage due to all the other $(i-1)$ tones is removed (with $k = 0, 1, \ldots, i$). This allows to progressively refine the amplitude, normalized Doppler frequency and normalized delay of each tone, so generating the final estimates. Note that, in principle, this re-estimation procedure can be repeated multiple (say, N_{REF}) times.

C. Computational Complexity of the Proposed Algorithms

The computational complexity, in terms of number of *floating point operations* (flops), can be assessed for both the CSFDE and the CSFDEC algorithms as follows.[12] First of all,

[12]The general criteria adopted in our evaluation of computational costs are summarised in [15, App. C].

the overall computational cost of the CSFDE is expressed as

$$\mathcal{C}_{\mathrm{CSFDE}} = \mathcal{C}_0(\mathrm{CSFDE}) + N_{\mathrm{it}}\,\mathcal{C}_i(\mathrm{CSFDE}), \tag{56}$$

where $\mathcal{C}_0(\mathrm{CSFDE})$ ($\mathcal{C}_i(\mathrm{CSFDE})$) represents the computational cost of its initialization (each of its iterations). The cost $\mathcal{C}_0(\mathrm{CSFDE})$ is evaluated by summing[13]: 1) the contribution due to the computation of the couple $(\hat{l}, \hat{p})$ on the basis of (43); 2) the contribution due to the computation of the matrices $\{\bar{\mathbf{Y}}_{k_1,k_2}\}$ on the basis of (33), including the evaluation of the spectrum $\bar{\mathbf{Y}}_{0,0}$; 3) the contributions due to the evaluation of the estimates $\hat{\Omega}$ and $\hat{\Delta}$, respectively, on the basis of the quadratic equation (34). The cost $\mathcal{C}_{i,\mathrm{CSFDE}}$, instead, is evaluated by summing: 1) the contribution due to the computation of $\bar{Y}(\hat{F}_D, \hat{F}_r)$ on the basis of (19) or of the interpolation of a few adjacent elements of the matrix $\bar{\mathbf{Y}}_s$ (29); 2) the contributions due to the evaluation of $\hat{\rho}_D$ ($\hat{\rho}_r$) on the basis of (46) ((47)); 3) the contribution due to the evaluation of $\hat{A}$ on the basis of (28); 4) the contribution due to the computation of the quantity $\bar{Y}_{k_1,k_2}(\hat{\rho}_D^{(i-1)}, \hat{\rho}_r^{(i-1)})$ (54) through the interpolation of a few adjacent elements of the matrix $L_D\,L_r\,\bar{\mathbf{Y}}_{k_1,k_2}$ (see (33)) for the considered values of (k_1, k_2); 5) the contributions due to the computation of $\hat{\Omega}$ and $\hat{\Delta}$ on the basis of (34). Based on these considerations and the mathematical results illustrated in [20, App. C], it can be proved that $\mathcal{C}_{\mathrm{CSFDE}} = \mathcal{O}(N_{\mathrm{CSFDE}})$, where

$$N_{\mathrm{CSFDE}} = 16\,M_0\,N_0\log_2(M_0\,N_0) + N_{\mathrm{it}}\,16\,I_D\,I_r \tag{57}$$

and I_D (I_r) is the interpolation order adopted in the Doppler (range) domain for the evaluation of $\bar{Y}_{k_1,k_2}(\hat{\rho}_D^{(i-1)}, \hat{\rho}_r^{(i-1)})$ (54). Note that, for small values of I_D and I_r (e.g., if a 2D linear or barycentric interpolation is used; see [19]), the contribution of the second term of the RHS of the last equation can be neglected, so that the order of the whole computational cost is well approximated by its first term, i.e. by the term originating from DSFT processing.

Our assessment of the complexity of the CSFDEC algorithm is based on the considerations illustrated in [15] for its 1D counterpart. Based on these, it can be proved that $\mathcal{C}_{\mathrm{CSFDEC}} = \mathcal{O}(N_{\mathrm{CSFDEC}})$, where

$$N_{\mathrm{CSFDEC}} = 16\,M_0\,N_0\log_2\left(M_0\,N_0\right) + K\,N_{\mathrm{it}}\;16\,I_D\,I_r, \tag{58}$$

so that the required computational effort depends *linearly* on K. The last result holds if *tone re-estimation* is not accomplished and all the tones are detected (i.e., $\hat{K} = K$). The first term appearing in the RHS of the last equation accounts for the initialization (and, in particular, for the computation of the matrices $\bar{\mathbf{Y}}_{0,0}$ (22) and $\{\bar{\mathbf{Y}}_{k_1,k_2}; (k_1, k_2) \neq (0,0)\}$ (33)), whereas the second one for the fact that, in the CSFDEC algorithm, the CSFDE is executed K times. Note that the computational cost related to the estimation of the 2D-tones detected after the first one and to their frequency domain cancellation does not play an important role in this case. However, if *tone re-estimation* is executed in the CSFDEC algorithm, the parameter K appearing in the RHS of (58) is replaced by K^2, since this task involves all the estimated 2D-tones.

[13]Note that the evaluation of the estimate of the tone complex amplitude is neglected, being based on (28), that requires a negligible computational effort.

D. Comparison of Our Multiple Tone Estimator With Related Techniques

The CSFDEC algorithm is conceptually related with: 1) the 2D *periodogram method* [6] (denoted 2D-FFT in the following); 2) the CLEAN algorithm [21], [22]; 3) the *modified Wax and Leshem* (MWL) algorithm developed in [21] and [22]. The 2D-FFT, CSFDEC and CLEAN algorithms are FFT-based techniques; however, the last two algorithms are more complicated than the first one. In fact, unlike the 2D-FFT, both the CSFDEC and CLEAN algorithms perform leakage compensation, iterative cancellation of the detected targets and tone re-estimation. Note also that the CLEAN algorithm, unlike the CSFDEC algorithm, does not accomplish fine frequency estimation and employs coarse frequency estimates in its target cancellation procedure. The MWL algorithm, similarly as the CSFDEC algorithm, relies on the idea of turning a complicated 3D optimization problem (see (13)) into a triplet of three simpler 1D optimization problems. However, unlike the CSFDEC algorithm, it requires the computation of orthogonal projections (and, consequently, of matrix inversions) and the definition of a search grid.

If frequency re-estimation is ignored, the following considerations can be formulated for the computational complexity of the above mentioned algorithms:

1) The computational effort of the CLEAN algorithm is expressed by the sum of three distinct contributions, related to its initialization (which is based on the 2D-FFT), its tone cancellation and its leakage compensation; these three costs are shared with the CSFDEC algorithm, that requires the computation of other 12 (or 15) additional DSFTs (see the previous subsection).

2) The CLEAN and MWL algorithms perform cancellation and leakage compensation in the *time domain*, whereas the CSFDEC algorithm performs these tasks in the *frequency domain*. This explains why the computational complexity of the CSFDEC cancellation, being in the order of $M_0 \times N_0$, is $L_D \times L_r$ times larger than the cost of the same task for the CLEAN and MWL algorithms.

3) The computational cost of leakage removal can be neglected for the CSFDEC algorithm because of its simplicity (complex scalar subtraction), even if it has to be accomplished on multiple DSFTs; on the other hand, the CLEAN and MWL algorithms execute this task in a similar fashion as cancellation, thus requiring $\mathcal{O}(M\,N)$ operations.

4) The computational effort of the MWL algorithm is expressed by the sum of two distinct contributions, one due to its initialization, the other one to its iterations. The cost of the initialization task is the same as that of the *Wax and Leshem* (WL) algorithm illustrated in [21]. The cost of each iteration, instead, is given by that of the WL algorithm plus a contribution due to leakage compensation; the last cost is $\mathcal{O}(K\,M\,N)$, being equal to that required by the CLEAN algorithm for the same procedure.

To sum up, the 2D-FFT is the least demanding algorithm; moreover, its computational effort is independent of the overall number of detected targets (i.e., of K). The MWL algorithm is less computationally demanding than the CLEAN algorithm since it exploits alternating maximization. The CSFDEC algorithm has the highest initialization cost and, usually, is computationally heavier than all the other algorithms mentioned above. However, the dependence of its complexity on K is limited and weaker than that exhibited by the CLEAN algorithm; in addition, the CSFDEC algorithm is substantially more accurate than all the other algorithms in the presence of multiple closely spaced targets, as shown in the following section.

IV. Numerical Results

The accuracy of the CSFDEC algorithm has been assessed in five different scenarios and compared with that achieved by the related algorithms introduced in Section III-D and four other algorithms, namely: 1) the 2D MUSIC algorithm [8], [9], [23]; 2) the approximate ML method recently proposed in [11] and dubbed *modified*[14] *alternating projection* ML (MAP-ML) algorithm; 3) an estimation algorithm based on the same 2D cost function as the MAP-ML algorithm, but not using the alternating projection method for its maximization (this algorithm is denoted *modified Zhang* ML, MZ-ML); 4) the *expectation maximization* (EM) algorithm. A detailed description of all these algorithms and an analysis of their computational complexity are provided in [20, Sec. IV], and are omitted here for space limitations; here, we limit to point out that the MAP-ML and MZ-ML algorithms require a significant computational effort, since they are ML-based and do not turn, unlike the CSFDEC and MWL algorithms, a multidimensional optimization problem into significantly simpler sub-problems.

In our work, the first three scenarios (denoted **S1**, **S2** and **S3**) are characterized by a couple of targets having amplitudes $A_0 = A_1 = 1$, but differ for the assumptions we make about their ranges and speeds. In fact, we have that: 1) in **S1**, the target ranges are $R_0 = 10$ m and $R_1 = 10 + 3R_{\rm bin}$ m, whereas the target velocities are $v_0 = 1.39$ m/s and $v_1 = 1.39 + 3v_{\rm bin}$ m/s (here, $R_{\rm bin} = c/(2N\Delta_f)$ and $v_{\rm bin} = c/(2M\, f_c\, T_s)$ represent the size of the range bin and velocity bin, respectively, that characterize our FFT processing in the absence of oversampling); 2) in **S2**, the range R_0 (velocity v_0) is uniformly distributed[15] over the interval $[R_{\min}, R_{\max}] = [3, 80]$ m ($[v_{\min}, v_{\max}] = [0.2778, 10]$ m/s), whereas $R_1 = R_0 + 1.1R_{\rm bin}$ and $v_1 = v_0 + 1.1v_{\rm bin}$; 3) in **S3**, the range R_0 (velocity v_0) is uniformly distributed over the interval $[R_{\min}, R_{\max}] = [3, 30]$ m ($[v_{\min}, v_{\max}] = [0.2778, 5.56]$ m/s), whereas $R_1 = R_0 + \Delta_R(d)\, R_{\rm bin}$ ($v_1 = v_0 + \Delta_v(d)\, v_{\rm bin}$), with $d = 0, 1, \ldots, 5$. In the last scenario, $\Delta_R(d) = 0.8 + 0.05\, d$ ($\Delta_v(d) = 0.8 + 0.05\, d$) represents the tone spacing normalized with respect to $R_{\rm bin}$ ($v_{\rm bin}$) and the *signal-to-noise ratio* (SNR), which, in general, is defined as SNR $\triangleq \sum_{k=0}^{K-1} |A_k|^2/\sigma_W^2$, is equal to 0 dB. The fourth scenario (denoted **S4**), instead, is characterized by $K \in \{2, 3, \ldots, 9\}$, i.e. by a varying number of targets. In addition, for any K, the amplitude, range and velocity of the kth target are given by $A_k \triangleq 10^{-k\Delta_a/10}$, $R_k \triangleq R_0 + 1.8\, k\, R_{\rm bin}$ and $v_k \triangleq v_0 + 1.8\, k\, v_{\rm bin}$, respectively (with $k = 0, 1, \ldots, K-1$), the random variables R_0 and v_0 are generated in the same way as **S3**, and the SNR is equal to 5 dB for the strongest tone. In the last scenario (denoted **S5**), the range and velocity of the kth target are generated according to the simple mathematical laws given for **S4**, but $R_{\rm bin} = v_{\rm bin} = 1.1$ and $A_k = 1$ for any k (with $K \in \{3, 5, 7, 9\}$) are assumed; moreover, the SNR ranges from -15 dB to 25 dB.

It is important to point out that: 1) in **S1** the spacing of the two targets in the velocity and range domains is fixed and not small, whereas in **S2** (**S3**) the spacing in both the range and velocity domains is small and fixed (variable); 2) **S4** is characterized by a variable number of close targets; 3) **S5** is characterized by a variable number of close targets and by a variable SNR; 4) in all the considered scenarios, positive velocities have been selected for all the targets and the overall number of targets has been assumed to be known.

In our computer simulations, the estimation accuracy of each algorithm has been assessed by evaluating the *root mean square error* (RMSE) for the range (RMSE$_R$) and velocity (RMSE$_v$) of the considered targets. Moreover, the following parameters have been selected for the OFDM modulation: 1) overall number of subcarriers $N = 32$; 2) overall number of OFDM symbols/frame $M = 32$; 3) subcarrier spacing $\Delta_f = 250$ kHz; 4) cyclic prefix duration $T_G = 12.5$ μs (consequently, the OFDM symbol duration is $T_s = 1/\Delta_f + T_G = 16.5$ μs); 5) carrier frequency $f_c = 78$ GHz; 6) cardinality of the PSK constellation $N_s = 32$. Then, we have that $R_{\rm bin} = 18.75$ m and $v_{\rm bin} = 3.64$ m/s.

In **S1** the accuracy of the all the considered estimation algorithms has been assessed. Moreover, the following choices have been made for these algorithms[16]: 1) the oversampling factor $L_D = 16$ ($L_r = 16$) has been chosen for Doppler (range) estimation in both the 2D-FFT and CSFDEC algorithms (so that $M_0 = ML_D = 512$ and $N_0 = NL_r = 512$; see (24) and (25), respectively); 2) (39) has been always employed in the evaluation of the CSFDEC residuals (so that 13 DSFTs $\{\bar{\mathbf{Y}}_{k_1,k_2}\}$ have been computed in each new run); 3) the 2D-FFT method has been used to compute the initial estimates of target range and Doppler in the MZML, MAP-ML and EM algorithms; 4) $M_0 = 512$ ($N_0 = 512$) has been chosen for the refinement grid over Doppler (range) employed by the CLEAN, MWL, MZML, MAP-ML and EM algorithms; 5) in the CSFDEC algorithm $N_{\rm it} = 15$ refinement steps have been accomplished for the computation of the range and Doppler residuals, the interpolation[17] orders $I_D = I_r = 7$ have been selected and $N_{\rm REF} = 3$ re-estimations have been executed; 6) $N_{\rm REF} = 5$ ($N_{\rm REF} = 3$) re-estimations have been

[14] In our work, the approximate ML-based algorithm devised in [11] has been properly modified to adapt it to our signal model (11) (that does not account for *inter-pulse* and *inter-subcarrier* Doppler effects).

[15] In both **S2** and **S3**, R_0 and v_0 are *independent* random variables.

[16] The values of the parameters (defined in detail in [20, Sec. IV]) selected for **S1** have been also employed in **S2** and **S3**.

[17] In all our simulations, the *barycentric interpolation* described in [19] has been always used.

executed by the CLEAN and MWL (MZML, MAP-ML and EM) algorithms; 7) $M_0 = N_0 = 11$ ($M_0 = N_0 = 9$) have been chosen for the grid size in the CLEAN and MWL (MZML, MAP-ML and EM) algorithms during the re-estimation steps; 8) a unit value has been assigned to all the *mixing coefficients* $\{\beta_k^{(i)}\}$ of the EM algorithm (see [20, Sec. IV, eq. (160)]); 9) the spacing between adjacent values in the search (initial search) grid for 2D-MUSIC algorithm (CLEAN and MWL algorithms) is $\Delta_R = 0.6$ m ($\Delta_v = 0.1166$ m/s). Moreover, in **S1**, $M_0 = 121$ ($N_0 = 121$) has been selected for the number of trial values of the 2D-MUSIC algorithm and for the initial trial values of the CLEAN and MWL algorithms in the Doppler (range) domain; such values are uniformly spaced in the range (velocity) interval[18] $[0, R_{\max}]$ ($[0, v_{\max}]$), with $R_{\max} = 72$ m ($v_{\max} = 13.986$ m/s).

Some numerical results referring to **S1** are given in Fig. 1, where the RMSE_R and RMSE_v characterizing all the considered algorithms is shown for SNR $\in [-15, 25]$ dB (in these figures and in all the following ones, simulation results are represented by labels, whereas continuous lines are drawn to ease reading). From these results it is easily inferred that:

1) The CSFDEC, CLEAN and MWL algorithms achieve good accuracy (very close to the CRLB) thanks to their use of cancellation and refinement procedures.

2) The RMSE curves for the 2D-FFT and 2D-MUSIC algorithms exhibit a floor at high SNRs.

3) The MAP-ML and the MZML algorithms perform similarly since both aim at maximizing the same cost function.

4) The EM algorithm can be fruitfully exploited to refine the estimates generated by other methods and, in particular, if employed jointly with the 2D-FFT algorithm, achieves an estimation accuracy similar to that provided by the MAP-ML and MZML algorithms.

As far as point 2) is concerned, it is worth pointing out that:

a) The accuracy of the 2D-FFT algorithm is intrinsically limited by the adopted FFT order, whereas that of the 2D-MUSIC algorithm by the discretization of its steering vector; for this reason, when the *spectral leakage* is limited (i.e., when the targets are well spaced), the RMSE achieved by these two algorithms at large SNRs is well approximated by the square root of the variance of a random variable uniformly distributed over an interval whose width is equal to the step size of the grid of the considered algorithm, i.e., to $\sqrt{(X_{\text{res}}^2/12)}$, with $X = R$ or v; here, $R_{\text{res}} = R_{\text{bin}}/N_0 = 1.171875$ m, $v_{\text{res}} = v_{\text{bin}}/M_0 = 0.2276$ m/s for the 2D-FFT, whereas $R_{\text{res}} = \Delta_R$ and $v_{\text{res}} = \Delta_v$ for the 2D-MUSIC).

b) For given values of M and N, the accuracy of the 2D-FFT algorithm improves if the associated oversampling factors increase; unluckily, oversampling can provide a limited improvement by itself, since it does not add extra information, but simply allows to interpolate adjacent spectral samples.

c) The accuracy of the 2D-MUSIC algorithm can be improved by selecting a finer grid, at the price, however, of an higher computational complexity, as shown in [20, Sec. IV-B].

d) Both the 2D-FFT and 2D-MUSIC algorithms do not execute refinement and/or re-estimation steps.

These considerations apply to all the following results shown for the two above mentioned algorithms.v In addition, in analyzing the results shown in Fig. 1, readers should keep in mind that: 1) the computational complexity of the CSFDEC (CLEAN) algorithm is approximately 17 (39) times higher than that of the 2D-FFT,[19] whereas that of the MWL algorithm is very close to it; 2) the complexity of the 2D-MUSIC, MAP-ML and MZML algorithms is 3481, 577 and 2593 times higher than that of the 2D-FFT algorithm, respectively; 3) the computational cost of the EM algorithm is approximately 149 (671) times smaller than that of the MAP-ML (MZML) algorithm.

Some numerical results referring to **S2** are provided in Fig. 2, where the RMSE_R and RMSE_v characterizing all the considered algorithms is shown for SNR $\in [-25, 20]$ dB. In this case, $M_0 = 131$ ($N_0 = 181$) have been selected for the number of trial values of the 2D-MUSIC algorithm and for the initial trial values of the CLEAN and MWL algorithms in the Doppler (range) domain; such values are uniformly spaced in the range (velocity) interval $[0, R_{\max}]$ ($[0, v_{\max}]$), with $R_{\max} = 108$ m ($v_{\max} = 15.15$ m/s). These results lead to the following conclusions:

1) The CSFDEC, MWL, CLEAN, MAP-ML, MZML and EM algorithms are substantially more accurate than the 2D-FFT and 2D-MUSIC techniques. In particular, the RMSEs in range (velocity) of the 2D-FFT and 2D-MUSIC algorithms are 3.9 (4) and 1.5 (1.68) times higher, respectively, than that of the above mentioned group of algorithms at SNR $= 0$ dB; moreover, these performance gaps, in terms of both RMSE_R and RMSE_v, tend to increase by a factor 1.75 if the SNR is incremented by 5 dB.

2) The trend of both the RMSE_R and RMSE_v curves referring to the 2D-MUSIC and 2D-FFT algorithms does not follow that of the corresponding CRLB; for this reason, these algorithms are ignored in following.

3) The SNR threshold of the CSFDEC, CLEAN, MAP-ML and EM algorithms is about -10 dB, whereas that of the MWL algorithm is substantially higher (about -5 dB).

4) The MAP-ML algorithm performs similarly as the MZML algorithm; however, since the latter estimator requires an higher computational effort than the former one, it is ignored in the following.

It is also important to point out that the considerations illustrated about the computational complexity of the various algorithms in **S1** still hold; however, the complexities of the CLEAN, 2D-MUSIC and MWL algorithms are 64, 5497 and 1.01 times higher than that of the 2D-FFT algorithm, respectively.

In **S3**, the RMSEs have been evaluated for different values of the normalized tone spacing Δ_R and Δ_v; some numerical results referring to this scenario are illustrated in Fig. 3, that shows the dependence of RMSE_R and RMSE_v, respectively,

[18]Note that, in our simulations, *positive* trial values are always considered for target velocities, without loss of generality.

[19]The 2D-FFT is taken as a reference since it represents the method commonly adopted in real world systems, thanks to its computational efficiency and acceptable accuracy.

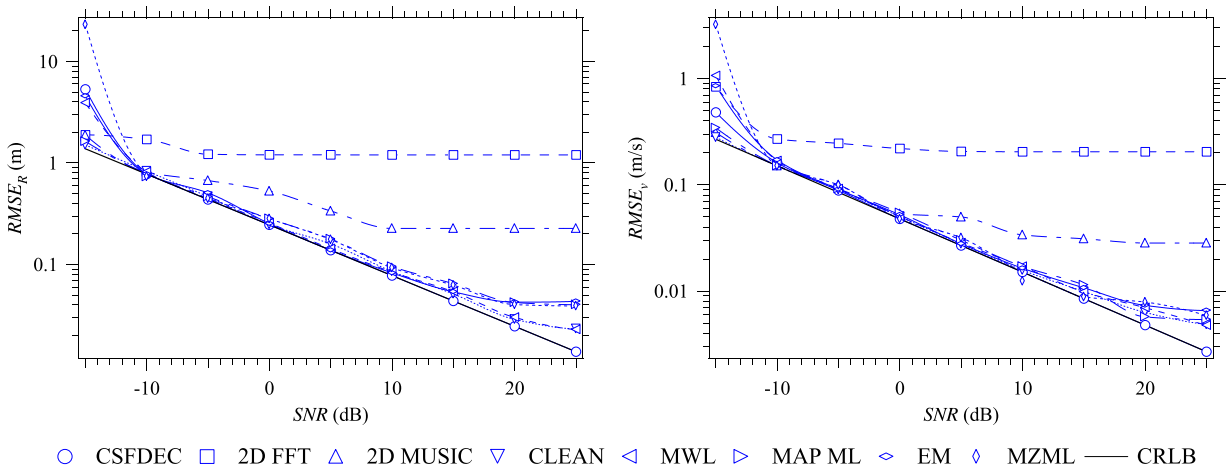

Fig. 1. Root mean square error performance achieved in range and velocity estimation (first scenario).

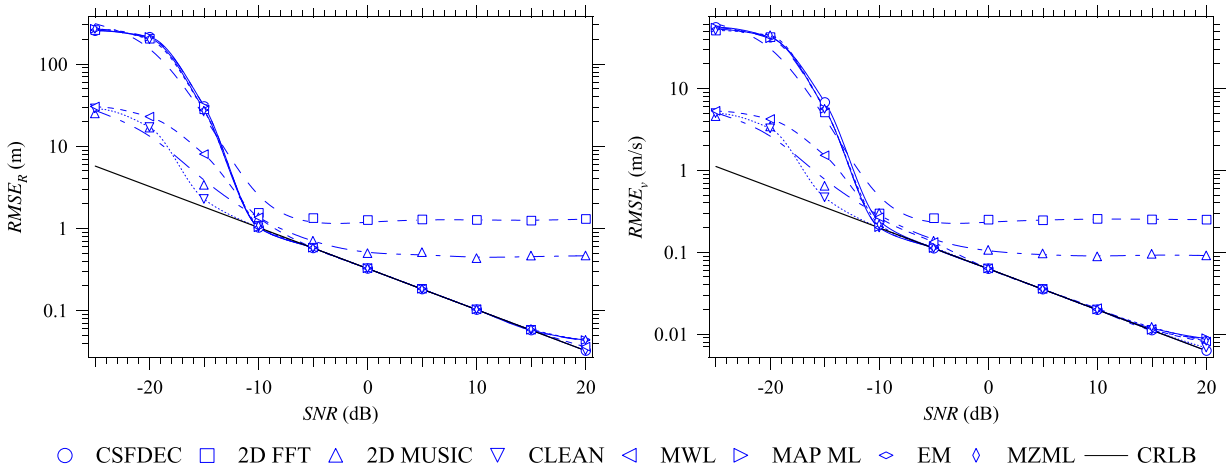

Fig. 2. Root mean square error performance achieved in range and velocity estimation (second scenario).

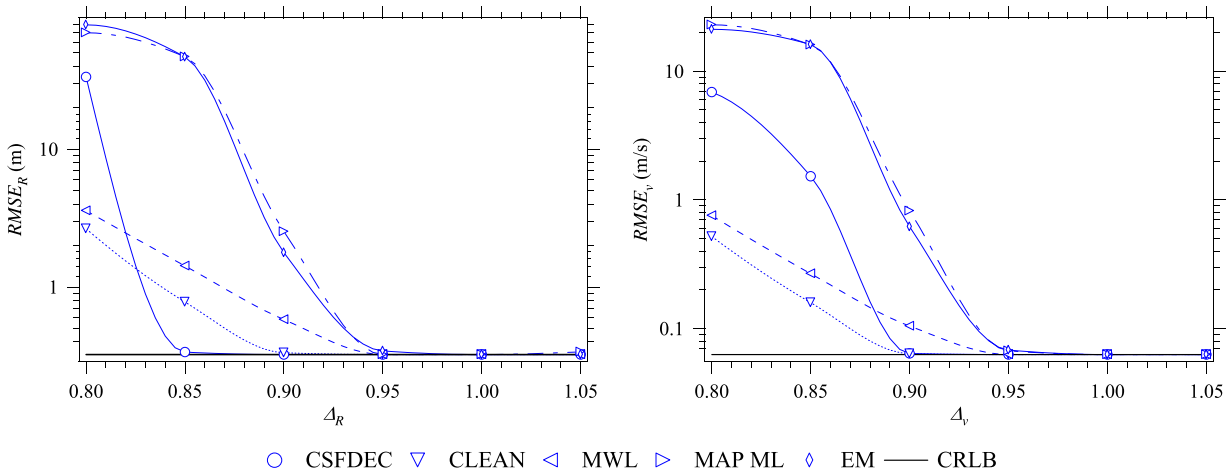

Fig. 3. Root mean square error performance achieved in range and velocity estimation (third scenario) for different values of the normalized tone spacing Δ_R and Δ_v, respectively. The CSFDEC, CLEAN, MWL, MAP-ML and EM algorithms are considered.

on the normalized tone spacing. In this case, the number of initial trial values are $M_0 = 101$ ($N_0 = 101$) for the CLEAN and MWL algorithms in the Doppler (range) domain; such values are uniformly spaced in the range (velocity) interval $[0, R_{\max}]$ ($[0, v_{\max}]$), with $R_{\max} = 60$ m ($v_{\max} = 11.66$ m/s). These results lead to the following conclusions: 1) The lowest threshold in range estimation is achieved by the CSFDEC algorithm (more specifically, in the considered scenario, its threshold is found at the normalized spacing $\Delta_R(2) = 0.9$); 2) the lowest threshold in velocity estimation is achieved by both the CLEAN and CSFDEC algorithms. Note also that the complexity of the CLEAN is approximately 1.6 times higher than that of the CSFDEC algorithm in this case.

Based on the considerations illustrated above, in **S4** we restrict our attention to the CSFDEC, CLEAN, MWL, MAP-ML and EM algorithms. Moreover, our performance analysis

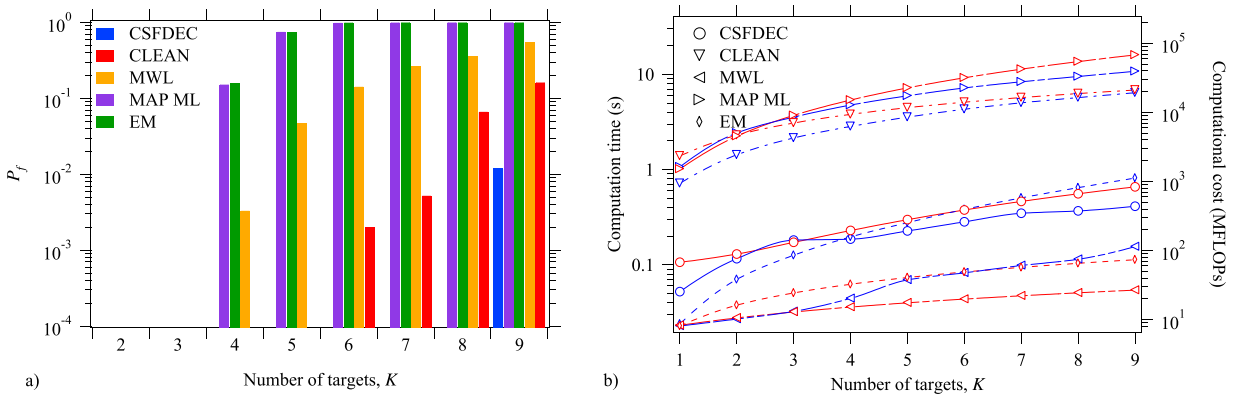

Fig. 4. a) Probability of failure versus overall number of tones; b) computational complexity in terms of computation time (blue curves) and computational cost (red curves). The CSFDEC, CLEAN, MWL, MAP-ML and EM algorithms are considered (fourth scenario).

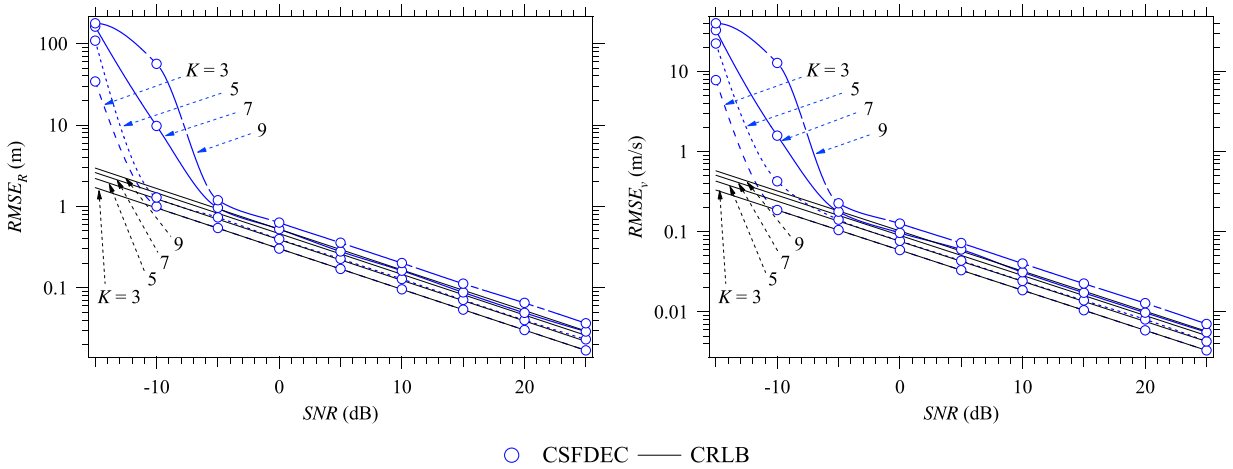

Fig. 5. Root mean square error performance achieved in range and velocity estimation (fifth scenario) by the CSFDEC algorithm with a varying number of targets, i.e. $K \in [3, 5, 7, 9]$ and the SNR $\in [-15; 25]$.

does not concern estimation accuracy, but the *probability of failure* (P_f), i.e. the probability that convergence is not achieved, so that large estimation errors can be generated. In our computer simulations, we have observed that large estimation errors occur more frequently as K increases. To detect the frequency of occurrence of these errors, we have counted, in each simulation run, the number of *failure events* for each of the considered algorithms; in practice, an event of this type is detected whenever the absolute value of the range error and that of the velocity error (or only one of these errors) exceed the thresholds $\Delta\epsilon_r = c/(4N\Delta_f) = 9.375$ m and $\Delta\epsilon_v = c/(4Mf_cT_s) = 1.82$ m/s, respectively.[20] Moreover, in generating our results for **S4**, the following changes have been made with respect to the previous scenarios: 1) $N_{\rm REF} = 7$ ($N_{\rm REF} = 5$) re-estimations have been executed by the CSFDEC, CLEAN and MWL (MAP-ML and EM) algorithms; 2) $M_0 = 551$ ($N_0 = 551$) have been selected for the initial trial values of the CLEAN and MWL algorithms in the Doppler (range) domain; 3) these trial values are uniformly spaced in the range (velocity) interval $[0, R_{\max}]$ ($[0, v_{\max}]$), with $R_{\max} = 330$ m ($v_{\max} = 64$ m/s). Note that the spacing between adjacent trial values is the same as **S1**-**S3** in both domains.

The probability of failure estimated for $K = 2, 3, \ldots, 9$ is illustrated in Fig. 4-a). From this figure it is easily inferred that: 1) the MAP-ML and EM (MWL) algorithms exhibit a P_f greater than 10^{-2} for $K \geq 4$ ($K \geq 5$); 2) the CSFDEC algorithm is substantially more robust than all the other algorithms since it is characterized by a P_f not exceeding 10^{-4} for $K \leq 8$; 3) the CLEAN algorithm achieves a P_f smaller than 10^{-2} for $K \leq 7$. These results evidence that the CSFDEC algorithm performs substantially better than the other estimators in the presence of multiple closely spaced targets. This feature plays a fundamental role in the estimation of extended targets, whose radar image is usually a dense point cloud.

In **S4** the computational effort required by the CSFDEC, CLEAN, MWL, MAP-ML and EM algorithms in terms of both *computation time* (CT)[21] and estimated number of *mega* FLOPs (MFLOPs) has been also evaluated. Our results, illustrated in Fig. 4-b), evidence that: 1) the MWL (MAP-ML) algorithm requires the lowest (highest) complexity in terms of both CT and MFLOPs; 2) the complexity of the CLEAN algorithm is not far from that of the MAP-ML algorithm; 3) the complexities of the CSFDEC and EM algorithms are comparable and placed in the middle.

[20]Note that $\Delta\epsilon_r$ ($\Delta\epsilon_v$) correspond to half the size of the range (Doppler) bin characterizing the processing of the considered algorithms.

[21]The CT has been assessed on a personal computer equipped with an i7 processor.

Our last results are shown in Fig. 5 and concern the RMSE_R and RMSE_v of the CSFDEC algorithm in **S5**; $N_{it} = 10$ and $N_{\text{REF}} = 3$ have been selected for this algorithm (the values of its remaining parameters are the same as **S1**). These results show that:

1) The SNR threshold of the CSFDEC algorithm depends on K; for instance, this threshold for the range estimation is found at a SNR ≈ -9 (SNR ≈ -5) dB for $K = 3$ and 5 ($K = 7$ and 9).

2) The range and velocity estimates generated by the CSFDEC algorithm are unbiased. Note, for instance, that for both $K = 7$ and 9, the RMSE_R and RMSE_v and the corresponding CRLB curves are separated by a constant SNR gap when the SNR exceeds the above mentioned threshold; further computer simulations have evidenced that this gap can be reduced by increasing the values of N_{REF} and, more evidently, of N_{it}, at the price, however, of an higher computational effort.

Finally, based on all the results illustrated above, we can state that, thanks to its accuracy, its limited complexity increase with respect to the 2D-FFT method and its ability to resolve multiple closely spaced point targets, the CSFDEC algorithm represents a good candidate for target detection and estimation in future OFDM-based radars.

V. Conclusion

In this manuscript, a novel algorithm for the detection of a single 2D complex tone and the estimation of its parameters has been derived. Moreover, it has been shown how combining this algorithm, dubbed CSFDE, with a serial cancellation procedure leads to the development of a new algorithm for the detection and the estimation of multiple 2D tones. Then, the last algorithm, called CSFDEC, has been applied to the detection of multiple targets, and to the estimation of their range and velocity in an OFDM-based SISO radar system. In addition, it has been compared, in terms of accuracy and computational complexity, with various estimation methods available in the technical literature. Our simulation results evidence that the CSFDEC algorithm is very accurate and outperforms all the other related estimators in the presence of multiple closely spaced targets. Future work concerns the application of the CSFDEC algorithm to other JCAS systems.

Appendix

A. Spectral Cancellation of a Two-Dimensional Complex Tone

In this paragraph, the derivation of expression of the vector $\bar{\mathbf{C}}_{0,0}(\cdot,\cdot,\cdot)$ appearing in the RHS of (51) is sketched. This vector is evaluated to cancel the contribution of the sequence

$$s_{m,n}\left(\bar{F}_D, \bar{F}_r, \bar{A}\right) = \bar{A}\,\bar{w}_D^m\,\bar{w}_r^n \tag{59}$$

to the vector $\bar{\mathbf{Y}}_{0,0}$ (22) (the adopted cancellation procedure is expressed by (50) and (51)); here, $\bar{w}_D \triangleq \exp(j2\pi\bar{F}_D)$ and $\bar{w}_r \triangleq \exp(-j2\pi\bar{F}_r)$. Since $\bar{\mathbf{Y}}_{0,0}$ is the order (M_0, N_0) DSFT of the zero-padded version $\hat{\mathbf{H}}_{0,0}^{(ZP)}$ (23) of the matrix $\hat{\mathbf{H}}_{0,0} = [\hat{H}_{m,n}]$, it is easy to show that

$$\bar{\mathbf{C}}_{0,0}\left(\bar{A}, \bar{F}_D, \bar{F}_r\right) = \bar{A}\,\bar{\mathbf{W}}_0, \tag{60}$$

where $\bar{\mathbf{W}}_0$ denotes the order (M_0, N_0) DSFT of the $M_0 \times N_0$ matrix

$$\bar{\mathbf{w}}_0 \triangleq \begin{bmatrix} \bar{\mathbf{w}} & \mathbf{0}_{M,N_0-N} \\ \mathbf{0}_{M_0-M,N} & \mathbf{0}_{M_0-M,N_0-N} \end{bmatrix}, \tag{61}$$

$\bar{\mathbf{w}} \triangleq [w_{m,n}]$ is an $M \times N$ matrix such that $w_{m,n} \triangleq \bar{w}^{m-n}$, with $m = 0, 1, \ldots, M-1$ and $n = 0, 1, \ldots, N-1$, and $\bar{w} \triangleq \bar{w}_D\,\bar{w}_r$. Then, the (m,n)th element of the matrix $\bar{\mathbf{W}}_0$ is given by

$$\begin{aligned} \bar{W}_0[m,n] &= \frac{1}{M_0}\sum_{l=0}^{M-1} \bar{w}_D^l \exp\left(-j2\pi\frac{m}{M_0}l\right) \\ &\quad \cdot \frac{1}{N_0}\sum_{p=0}^{N-1} \bar{w}_r^p \exp\left(j2\pi\frac{n}{N_0}p\right) \\ &= \frac{1}{M_0}\sum_{l=0}^{M-1} \left(\hat{q}_D[m]\right)^l \frac{1}{N_0}\sum_{p=0}^{N-1} \left(\hat{q}_r[n]\right)^p, \end{aligned} \tag{62}$$

where $\hat{q}_D[m] \triangleq \exp(j2\pi(\hat{F}_D - m/M_0))$ and $\hat{q}_r[m] \triangleq \exp(-j2\pi(\hat{F}_r - n/N_0))$. Note that the identity in [20, App. A, eq. (173)] can be exploited for an efficient computation of the two sums appearing in the RHS of (62).

B. Cancellation of Two-Dimensional Spectral Leakage

In this paragraph, the expression of the quantity $\bar{Y}_{k_1,k_2}(\cdot\,,\cdot;\cdot,\cdot,\cdot)$ appearing in the RHS of (53) and (55) is derived. This quantity is computed by the CSFDEC algorithm to cancel the contribution of the sequence $\{s_{m,n}(\bar{F}_{D_k}, \bar{F}_{r_k}, \bar{A}_k)\}$ (see (59)) to $\bar{Y}_{k_1,k_2}^{(i)}(\rho_D^{(i)}, \rho_r^{(i)})$ (54) for $k_1, k_2 = 0, 1, 2, 3$. It is not difficult to show that

$$\begin{aligned} &\bar{Y}_{k_1,k_2}\left(\hat{F}_{D,c_i}^{(i)}, \hat{F}_{r,c_i}^{(i)}; \hat{A}_k^{(i-1)}, \hat{F}_{D_k}^{(i-1)}, \hat{F}_{r_k}^{(i-1)}\right) \\ &\quad = \bar{A}_k^{(i-1)}\,\bar{W}_{k_1k_2}^{(k)}\left(\hat{F}_{D,c_i}^{(i)}, \hat{F}_{r,c_i}^{(i)}; \hat{F}_{D_k}^{(i-1)}, \hat{F}_{r_k}^{(i-1)}\right), \end{aligned} \tag{63}$$

where

$$\begin{aligned} &\bar{W}_{k_1k_2}^{(k)}\left(\hat{F}_{D,c_i}^{(i)}, \hat{F}_{r,c_i}^{(i)}; \hat{F}_{D_k}^{(i-1)}, \hat{F}_{r_k}^{(i-1)}\right) \\ &\quad = \frac{1}{M_0}\sum_{m=0}^{M-1} m^{k_1}\left(\bar{q}_D\left(\hat{F}_{D,c_i}^{(i)}, \hat{F}_{D_k}^{(i-1)}\right)\right)^m \\ &\qquad \cdot \frac{1}{N_0}\sum_{n=0}^{N-1} n^{k_2}\left(\bar{q}_r\left(\hat{F}_{r,c_i}^{(i)}, \hat{F}_{r_k}^{(i-1)}\right)\right)^n, \end{aligned} \tag{64}$$

with $\bar{q}_D(\hat{F}_{D,c_i}^{(i)}, \hat{F}_{D_k}^{(i-1)}) \triangleq \exp(j2\pi(\hat{F}_{D_k}^{(i-1)} - \hat{F}_{D,c_i}^{(i)}))$, $\bar{q}_r(\hat{F}_{r,c_i}^{(i)}, \hat{F}_{r_k}^{(i-1)}) \triangleq \exp(-j2\pi(\hat{F}_{r_k}^{(i-1)} - \hat{F}_{r,c_i}^{(i)}))$; here $\hat{F}_{D_k}^{(i-1)}$ and $\hat{F}_{r_k}^{(i-1)}$ are the *fine estimates* of the normalized Doppler frequency and normalized delay, respectively, computed at the $(i-1)$th iteration for the kth target. Note that the identities in [20, eqs. (173) and (178)-(180)] can be exploited for an efficient computation of all the factors appearing in the RHS of (53) and (54) (with $k_1, k_2 = 0, 1, 2, 3$).

References

[1] J. A. Zhang et al., "An overview of signal processing techniques for joint communication and radar sensing," *IEEE J. Sel. Topics Signal Process.*, vol. 15, no. 6, pp. 1295–1315, Nov. 2021.

[2] K. V. Mishra, M. R. B. Shankar, V. Koivunen, B. Ottersten, and S. A. Vorobyov, "Toward millimeter-wave joint radar communications: A signal processing perspective," *IEEE Signal Process. Mag.*, vol. 36, no. 5, pp. 100–114, Sep. 2019.
[3] L. Zheng and X. Wang, "Super-resolution delay-Doppler estimation for OFDM passive radar," *IEEE Trans. Signal Process.*, vol. 65, no. 9, pp. 2197–2210, May 2017.
[4] C. Sturm and W. Wiesbeck, "Waveform design and signal processing aspects for fusion of wireless communications and radar sensing," *Proc. IEEE*, vol. 99, no. 7, pp. 1236–1259, Jul. 2011.
[5] S. Mercier, S. Bidon, D. Roque, and C. Enderli, "Comparison of correlation-based OFDM radar receivers," *IEEE Trans. Aerosp. Electron. Syst.*, vol. 56, no. 6, pp. 4796–4813, Dec. 2020.
[6] Y. L. Sit, C. Sturm, and T. Zwick, "Doppler estimation in an OFDM joint radar and communication system," in *Proc. German Microw. Conf.*, Mar. 2011, pp. 1–4.
[7] S. Mercier, D. Roque, S. Bidon, and C. Enderli, "Correlation-based radar receivers with pulse-shaped OFDM signals," in *Proc. IEEE Radar Conf. (RadarConf)*, Florence, Italy, Sep. 2020, pp. 1–6.
[8] R. Xie, D. Hu, K. Luo, and T. Jiang, "Performance analysis of joint range-velocity estimator with 2D-MUSIC in OFDM radar," *IEEE Trans. Signal Process.*, vol. 69, pp. 4787–4800, 2021.
[9] Y. Liu, G. Liao, Y. Chen, J. Xu, and Y. Yin, "Super-resolution range and velocity estimations with OFDM integrated radar and communications waveform," *IEEE Trans. Veh. Technol.*, vol. 69, no. 10, pp. 11659–11672, Oct. 2020.
[10] F. Zhang, Z. Zhang, and W. Yu, "Joint range and Doppler estimation with amplitude weighted linearly constrained minimum variance method for OFDM-based RadCom systems," in *Proc. IEEE Radar Conf. (RadarConf)*, Florence, Italy, Sep. 2020, pp. 1–6.
[11] F. Zhang, Z. Zhang, W. Yu, and T.-K. Truong, "Joint range and velocity estimation with intrapulse and intersubcarrier Doppler effects for OFDM-based RadCom systems," *IEEE Trans. Signal Process.*, vol. 68, pp. 662–675, 2020.
[12] U. K. Singh, R. Mitra, V. Bhatia, and A. K. Mishra, "Target range estimation in OFDM radar system via kernel least mean square technique," in *Proc. Int. Conf. Radar Syst. (Radar)*, Oct. 2017, pp. 1–5.
[13] A. E. Assaad, M. Krug, and G. Fischer, "Distance and vehicle speed estimation in OFDM multipath channels," in *Proc. 21st Int. Conf. Microw., Radar Wireless Commun. (MIKON)*, May 2016, pp. 1–5.
[14] J. Fink, M. Braun, and F. K. Jondral, "Effects of arbitrarily spaced subcarriers on detection performance in OFDM radar," in *Proc. IEEE Veh. Technol. Conf. (VTC Fall)*, Sep. 2012, pp. 1–5.
[15] P. D. Viesti, A. Davoli, G. Guerzoni, and G. M. Vitetta, "Recursive algorithms for the estimation of multiple superimposed undamped tones and their application to radar systems," *IEEE Trans. Aerosp. Electron. Syst.*, vol. 59, no. 2, pp. 1834–1853, Apr. 2023.
[16] I. Ziskind and M. Wax, "Maximum likelihood localization of multiple sources by alternating projection," *IEEE Trans. Acoust., Speech, Signal Process.*, vol. ASSP-36, no. 10, pp. 1553–1560, Oct. 1988.
[17] D. Rife and R. Boorstyn, "Single tone parameter estimation from discrete-time observations," *IEEE Trans. Inf. Theory*, vol. IT-20, no. 5, pp. 591–598, Sep. 1974.
[18] E. Isaacson and H. B. Keller, *Analysis Of Numerical Methods*. New York, NY, USA: Dover, 1994.
[19] J.-P. Berrut and L. N. Trefethen, "Barycentric Lagrange interpolation," *SIAM Rev.*, vol. 46, no. 3, pp. 501–517, Jan. 2004.
[20] M. Mirabella, P. D. Viesti, A. Davoli, and G. M. Vitetta, "An approximate maximum likelihood method for the joint estimation of range and Doppler of multiple targets in OFDM-based radar systems," *TechrXiv*, Jul. 2022. [Online]. Available: https://www.techrxiv.org/articles/preprint/An_Approximate_Maximum_Likelihood_Method_for_the_Joint_Estimation_of_Range_and_Doppler_of_Multiple_Targets_in_OFDM-Based_Radar_Systems/20296896
[21] E. Sirignano, A. Davoli, G. M. Vitetta, and F. Viappiani, "A comparative analysis of deterministic detection and estimation techniques for MIMO SFCW radars," *IEEE Access*, vol. 7, pp. 129848–129861, 2019.
[22] A. Davoli, E. Sirignano, and G. M. Vitetta, "Three-dimensional deterministic detection and estimation algorithms for MIMO SFCW radars," in *Proc. IEEE Radar Conf. (RadarConf)*, Florence, Italy, Sep. 2020, pp. 1–6.
[23] C. R. Berger, B. Demissie, J. Heckenbach, P. Willett, and S. Zhou, "Signal processing for passive radar using OFDM waveforms," *IEEE J. Sel. Topics Signal Process.*, vol. 4, no. 1, pp. 226–238, Feb. 2010.

Michele Mirabella (Graduate Student Member, IEEE) received the B.S. and M.S. degrees (cum laude) in electronic engineering from the University of Modena and Reggio Emilia, Italy, in 2019 and 2021, respectively, where he is currently pursuing the Ph.D. degree. His research interests include joint communication and sensing systems.

Pasquale Di Viesti (Graduate Student Member, IEEE) received the bachelor's and master's degrees (cum laude) in electronic engineering from the University of Modena and Reggio Emilia, Italy, in 2016 and 2018, respectively, and the Ph.D. degree in automotive for an intelligent mobility from the University of Bologna in October 2021. He is currently a Post-Doctoral Research Fellow with the University of Modena and Reggio Emilia. His research interests include statistical signal processing and MIMO radars.

Alessandro Davoli (Graduate Student Member, IEEE) received the B.S. and M.S. degrees (cum laude) in electronic engineering from the University of Modena and Reggio Emilia, Italy, in 2016 and 2018, respectively, and the Ph.D. degree in automotive for an intelligent mobility from the University of Bologna in October 2021. His research interests include MIMO radars, with emphasis on the development of novel detection and estimation algorithms for automotive applications.

Giorgio M. Vitetta (Senior Member, IEEE) received the Dr.Ing. degree (cum Laude) in electronic engineering and the Ph.D. degree from the University of Pisa, Italy, in 1990 and 1994, respectively. Since 2001, he has been a Full Professor of telecommunications with the University of Modena and Reggio Emilia. He has coauthored more than 100 papers published on international journals and on the proceedings of international conferences, and has coauthored the book *Wireless Communications: Algorithmic Techniques* (John Wiley, 2013). His research interests include wireless and wired data communications, localization systems, MIMO radars, and the smart grids. He served as the Area Editor for the IEEE TRANSACTIONS ON COMMUNICATIONS and the Associate Editor for the IEEE WIRELESS COMMUNICATIONS LETTERS and the IEEE TRANSACTIONS ON WIRELESS COMMUNICATIONS.

Open Access funding provided by 'Università degli Studi di Modena e Reggio Emilia' within the CRUI CARE Agreement